DOT/FAA/PM-84/15

Project Report
ATC-129

A Gust Front Case Studies Handbook

Diana L. Klingle

10 January 1985

Lincoln Laboratory
MASSACHUSETTS INSTITUTE OF TECHNOLOGY
LEXINGTON, MASSACHUSETTS

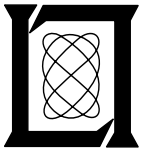

Prepared for the Federal Aviation Administration,
Washington, D.C. 20591

TECHNICAL REPORT DOCUMENTATION PAGE

1. Report No.	2. Government Accession No.	3. Recipient's Catalog No.
DOT/FAA/PM-84/15		

4. Title and Subtitle	5. Report Date
A Gust Front Case Studies Handbook	10 January 1985
	6. Performing Organization Code

7. Author(s)	8. Performing Organization Report No.
Diana L. Klingle	ATC-129

9. Performing Organization Name and Address	10. Work Unit No. (TRAIS)
Purdue University Dept. of Geosciences W. Lafayette, IN	11. Contract or Grant No. DT-FA01-80-Y-10546
	13. Type of Report and Period Covered
12. Sponsoring Agency Name and Address Department of Transportation Federal Aviation Administration Systems Research and Development Service Washington, D.C. 20591	Project Report
	14. Sponsoring Agency Code

15. Supplementary Notes

The work reported in this document was performed at the National Severe Storms Laboratory under MIT/Lincoln Laboratory grant number CX-5013.

16. Abstract

Gust fronts produce low altitude wind shear that can be hazardous to aircraft operations, especially during takeoff and landing. Radar meterologists have long been able to identify gust front signatures in Doppler radar data, but in order to use the radars efficiently, automatic detection of such hazards is essential.

Eight gust front case studies are presented. The data include photographs of the Doppler weather radar displays, thermodynamic and wind measurements from a 440 m high tower, environmental soundings and tables of gust front characteristics. The tabulated characteristics are those thought to be most important in developing rules for automatic gust front detection such as length and height, maximum and minimum values of reflectivity, velocity and spectrum width, and estimates of radial shear. For the cases studied, outflows could be detected most reliably in the velocity field, but useful information also could be gleaned from the spectrum width and reflectivity fields. The signal-to-noise ratio threshold was found to be a major factor in the ability of an observer to discern the gust front signature in the Doppler radar displays. Detection within the spectrum width field required a higher SNR than did the radial velocity field.

17. Key Words	18. Distribution Statement
Doppler Weather Radar gust fronts low altitude wind shear aviation weather hazards	Document is available to the public through the National Technical Information Service, Springfield, Virgina 22161.

19. Security Classif. (of this report)	20. Security Classif. (of this page)	21. No. of Pages	22. Price
Unclassified	Unclassified	122	

Form DOT F 1700.7 (8-69)

ABSTRACT

Gust fronts produce low altitude wind shear that can be hazardous to aircraft operations, especially during takeoff and landing. Radar meteorologists have long been able to identify gust front signatures in Doppler radar data, but in order to use the radars efficiently, automatic detection of such hazards is essential.

Eight gust front case studies are presented. The data include photographs of the Doppler weather radar displays, thermodynamic and wind measurements from a 440 m high tower, environmental soundings and tables of gust front characteristics. The tabulated characteristics are those thought to be most important in developing rules for automatic gust front detection such as length and height, maximum and minimum values of reflectivity, velocity and spectrum width, and estimates of radial shear. For the cases studied, outflows could be detected most reliably in the velocity field, but useful information also could be gleaned from the spectrum width and reflectivity fields. The signal-to-noise ratio threshold was found to be a major factor in the ability of an observer to discern the gust front signature in the Doppler radar displays. Detection within the spectrum width field required a higher SNR than did the radial velocity field.

ACKNOWLEDGMENTS

The author wishes to specially thank M. Wolfson at MIT/Lincoln Laboratory for suggesting this study, for providing support and ideas throughout the course of this research, and for assisting in the final editing and production of this report.

I also want to express my sincere gratitude to all those at NSSL who gave so generously of their valuable time. In particular, I wish to thank Drs. Zrnic' and Uyeda for their helpful comments and for the use of their Convergence algorithm, Messrs. Lee, Eilts and Thomas for use of the tower data and related plotting programs, and Mr. Showell for the soundings. Thanks also to Dr. E. Kessler for allowing me the opportunity to work at NSSL and use the Doppler data sets and to Dr. J. Evans at MIT/Lincoln Laboratory and Dr. David Smith at Purdue University for sharing their ideas and editorial comments. Appreciation is extended to V. Ewing, M. Dalpe' and B. Farino for their patience in typing various drafts of this manuscript.

ACRONYMS AND ABBREVIATIONS

AGL - Above Ground Level

AWS - U.S. Air Force Weather Service (Air Weather Service)

CST - Central Standard Time

EDM - Edmond, OK rawinsonde site

FAA - Federal Aviation Administration

km - kilometers

ms^{-1} - meters per second

NEXRAD - Next Generation Doppler Weather Radar

NRO - Norman, OK Doppler radar site

NSSL - National Severe Storms Laboratory

NWS - National Weather Service

OKC - Oklahoma City, OK rawinsonde site

OUN - Norman, OK rawinsonde site

PPI - Plan Position Indicator

PRF - Pulse Repetition Frequency

SNR - Signal-to-Noise Ratio

ST - Signal-to Noise Ratio Threshold

TTS - Tuttle, OK rawinsonde site

CONTENTS

APPENDICES

List of Illustrations

List of Tables

I. INTRODUCTION

A gust front is the boundary between the horizontally propagating cold air outflow from a thunderstorm and the surrounding environmental air. The sharp changes in both horizontal and vertical wind speed and direction across the front can be hazardous to aircraft on takeoffs and landings. Turbulence created at the boundary can also impact aircraft operations. Gust fronts, as well as downbursts and tornadic phenomena, constitute an aviation hazard but it is not possible to detect the low altitude wind shear they produce with the conventional radars currently in use. However, the Federal Aviation Administration (FAA), National Weather Service (NWS), and U.S. Air Force Weather Service (AWS) are jointly funding a nationwide network of Doppler weather radars (NEXRAD) capable of sensing air motions. In order to use the Doppler radars efficiently, automatic detection of weather hazards is essential.

Doppler radar data have been recorded on a number of gust fronts. Although radar meteorologists are usually able to detect gust front signatures, attempts to automatically detect them based on Doppler radar data have had limited success. One reason for this may be that typically only one or two case studies have been used to determine detectable, characteristic signatures of the thunderstorm outflow.

This report represents a collection of gust front case studies performed using Doppler data collected by the National Severe Storms Laboratory (NSSL) at Norman, OK. Eight gust front cases are presented (30 April 1978, 2 May 1978, 19 June 1980, 15 May 1982, 30 May 1982, 17 May 1983, 10 June 1983, and 26 April 1984). These cases were chosen because they illustrate the gust front signatures in the three-moment displays, they demonstrate the difficulties of detecting gust fronts in radar data, and they represent a cross-section of typical gust front types. Tabulated results gathered from the single Doppler radar data include length and height of the gust front; maximum, minimum, and average values of Doppler velocity, spectrum width, and radial shear; and overall gust front pattern.

Whenever possible, data from the WKY-TV instrumented tower and prestorm soundings were acquired. The WKY-TV tower, which is located 35 to 40 km north of the Norman Doppler radar (NRO), is instrumented to a height of about 440 m. At this distance (assuming an elevation angle of 0.5°), the center of the NRO beam is at a height of 350 m. Thus, tower data can be used to determine the outflow structure in the lowest levels and verify Doppler winds at the lowest elevation angles. Soundings are provided in order to illustrate the environmental conditions (winds and thermodynamic stability) within which the storms and gust fronts formed and propagated.

Throughout this report meteorological terms are used freely and, in most cases, without definition. Appendix D contains a list of these meteorological terms and the definitions.

II. BACKGROUND ON GUST FRONTS

A. Gust Front Structure

A gust front is the leading edge of an outflow which is produced when the thunderstorm downdraft reaches the ground and spreads horizontally. The vertical velocities within the downdraft cannot be measured by the Doppler radar at low elevation angles, but as the outflow spreads, a divergent signature can be identified in the Doppler wind field. The passage of a gust front is often accompanied by a sharp rise in pressure, a decrease in temperature, and abrupt changes in wind speed and direction. As the cooler, denser outflow intrudes into the warm, less dense environmental air, the warm air is lifted up and over the outflow boundary. Figure II-1 is a photograph of the arcus cloud formed by this lifting of warm, moist air by an approaching gust front. The intrusion of cooler air into warmer has been likened to a gravity current (Benjamin, 1968; Goldman and Sloss, 1969; Simpson, 1969; Charba and Sasaki, 1971).

Studies of laboratory gravity currents have illustrated the presence of phenomena which have counterparts in thunderstorm outflows. Fluid within the outflow moves faster than the outflow boundary. Under the proper conditions friction between the fluid and the surface across which it propagates causes the lowest layers of the flow to be retarded. Fluid within this layer is deflected downward, producing "backflow". The fluid above this friction layer moves faster and protrudes ahead of the surface boundary. This protrusion is known as the "nose" of the gust front (Fig. II-2). The advancing fluid is deflected upward at the leading edge producing a bulge known as the "head". A turbulent "wake" region is located behind the head, where mixing of the outflow and environmental air occurs. Since the outflow interface is not an impermeable boundary, mixing also occurs along the leading edge. Studies have shown evidence that these features also exist in nature (e.g., Charba, 1972; Goff, 1975).

B. Doppler Radar Signatures of Gust Fronts

It has been shown that Doppler radar is capable of detecting thunderstorm outflows (e.g., Brandes, 1976, Lee, et. al., 1978; Wakimoto, 1982). The abrupt change in wind speed and direction mentioned previously can be sensed by the Doppler radar and displayed such that regions of radial convergence (radial shear) are apparent. Zrnic' and Lee (1983), henceforth referred to as Z-L, outline some of the difficulties which may prevent gust front detection by radar. For instance, the distance of the center of the radar beam above the surface increases with distance from the radar. A shallow outflow at a large distance from the radar may be below the beam, and thus go undetected. Near the radar, ground clutter contaminates the signal. Range folding (i.e., targets beyond the unambiguous range appear to be located within the first trip) can mask the gust frontal signature. Despite these problems, gust fronts can generally be detected in the Doppler data at ranges up to 100 km.

Fig. II-1. Arcus cloud associated with an approaching Oklahoma gust front. This feature is formed as the warm moist environmental air is forced aloft at the leading edge of the outflow.

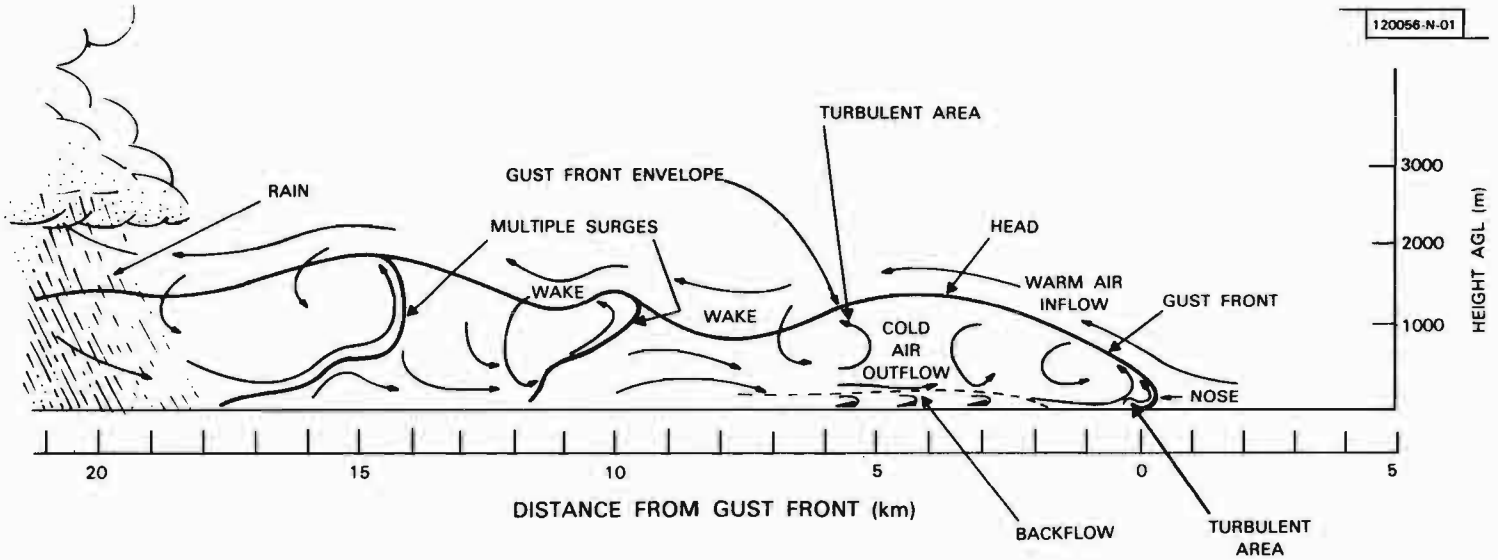

Fig. II-2. Schematic diagram of the vertical structure of a thunderstorm outflow and gust front. Motion is gust front relative. (Adapted from Goff, 1976.)

1. Reflectivity

Gust fronts are often associated with "thin line" echoes in radar reflectivity fields. Strong gradients in the refractive index at the leading edge of the outflow were sited as a possible explanation of this phenomena (e.g., Leach 1957; Luckenback 1958, Brown 1960). Others, including Harper (1958, 1960), believed the thin line was caused by insects which were picked up and carried along by the outflow and by birds that fed upon these insects. More recently, Wakimoto (1982) suggested that the thin line was produced by the "precipitation roll", that is, by precipitation particles which were swept along with the outflow winds as they moved away from the parent storm. Figure II-3 illustrates the typical stages in the life cycle of a gust front and the precipitation roll.

2. Doppler Velocity

Gust fronts can be identified in the Doppler wind field as linear patterns of radial shear. Shear is the change in velocity over a given distance. Since velocity is a vector quantity, shear can be associated with a change in speed and/or a change in direction. As an example, assume a gust front is approaching the radar from the west. A reasonable first approximation is that winds within the outflow are oriented perpendicular to the gust front and therefore have a strong radially inbound component in regions where the gust front is perpendicular to the beam (Fig. II-4). Environmental winds ahead of the gust front are typically from the southeast to southwest quadrant in Oklahoma and display outbound (+) or weak inbound (-) velocities. Moving away from the radar toward the gust front along a radial, one finds the Doppler velocities changing from positive (or weak negative) to negative (or more strongly negative) as the gust front is encountered. This abrupt change in Doppler wind speed produces a linear radial shear signature at the leading edge of the outflow.

The gust front tends to curve (Fig. II-4) and portions of its length may become aligned along a radial. When this occurs, the flow is primarily across the beam and as such is sensed as zero velocity by the Doppler radar. Identifying the radially-oriented portions of the gust front in the radar velocity field can be difficult.

3. Spectrum Width

Occasionally, gust fronts appear as linear patterns of broadened Doppler velocity spectra (Z-L). The outflow leading edge where lifting and mixing occur and the wake region behind the head have been identified as turbulent areas and should therefore be associated with widened velocity spectra.

Unfortunately, the gust front is not the only cause of enhanced spectrum width. A broadening of the velocity spectra is also associated

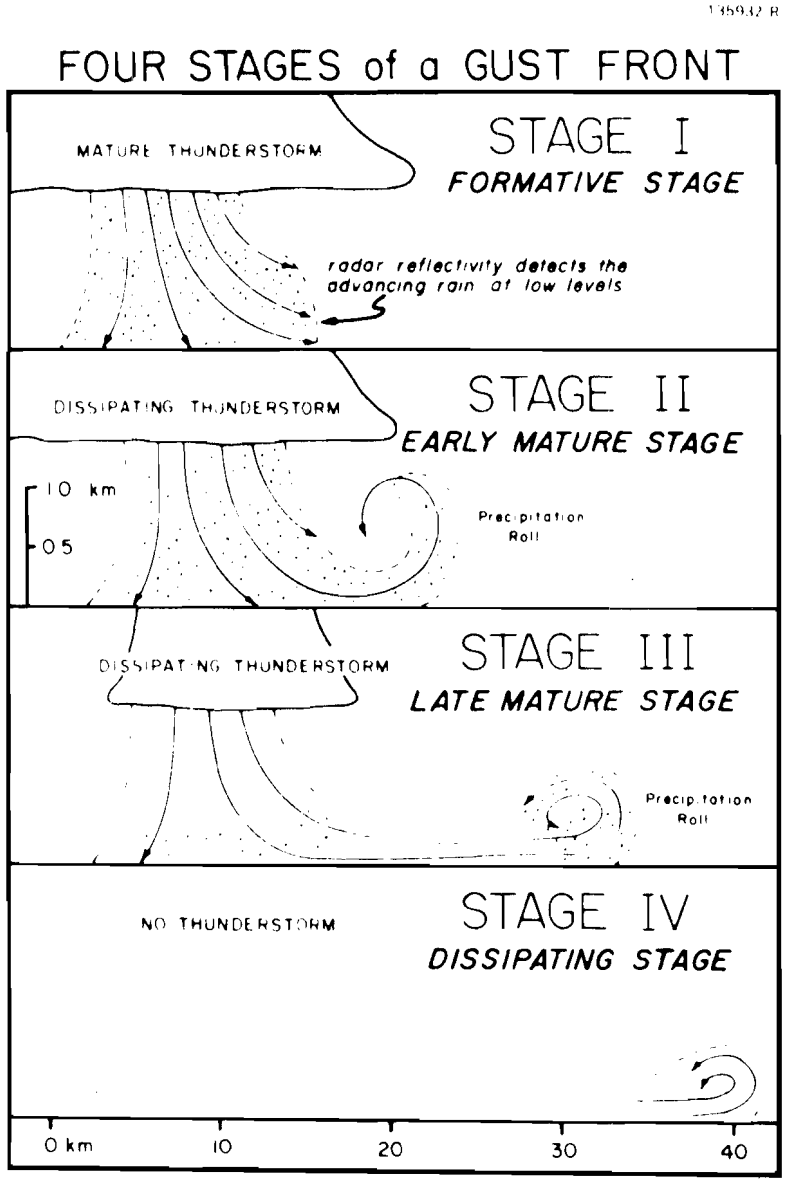

Fig. II-3. Life cycle of the gust front (vertical cross section). Note the formation of the "precipitation roll" which is believed to produce the thin line echo.

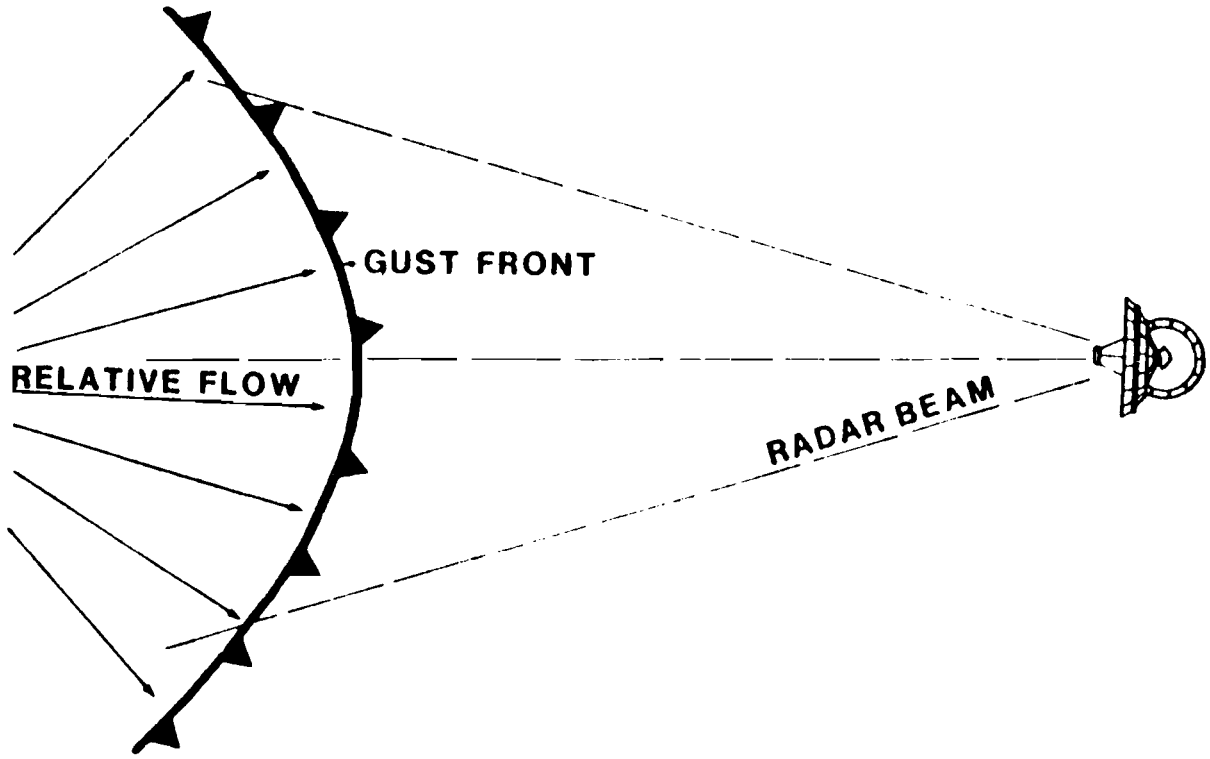

Fig. II-4. Schematic diagram of the horizontal structure of a thunderstorm outflow and gust front. Winds within the outflow tend to flow perpendicular to the gust front. The dashed lines indicate possible locations of a radar beam which scans the outflow.

with regions of weak signal. As the signal-to-noise ratio decreases, the signal due to weather approaches the noise level and the estimated spectrum widths are effectively those of noise.

Enhanced spectrum widths are often found at the edges of cell echoes where the signal strength is decreasing. This may simply be due to the low signal-to-noise ratio but it could be due to the presence of real turbulence. The echo edge is not a solid boundary. Mixing of the drier environmental air and moister thunderstorm air leads to evaporation of water droplets and cooling, which in turn produces downdrafts, updrafts and turbulence.

Doppler velocity spectra also appear to broaden around areas of range aliasing or range folding. Figure II-5 illustrates how echoes beyond the unambiguous range or first trip can lead to obscuration of first trip weather signals. If the folded signals overlap weather located within the first trip, then the velocity spectra are superimposed and the parametric estimates of spectrum width may be erroneous.

At NSSL, identification of these range folded areas is accomplished by using a dual PRF which allows for two different unambiguous ranges. The lower PRF is used for the reflectivity estimates which have one-fourth the resolution, but four times the unambiguous range of the Doppler estimates. If the first trip (Doppler) echo is not 10 dB greater than echoes from successive trips, data in the region of overlap are not displayed. It will be shown in section IV of this report that large spectrum widths are found around the perimeter of these range folded areas. It may be that as the signal from successive trip echoes decreases (e.g., at echo edges), the 10 dB threshold is exceeded and erroneous spectrum width values resulting from the overlap are displayed. Examples of this will be noted later.

Zrnic' and Lee (1983) collected and tabulated data from eight gust front cases. Their work served as a basis for this research. Many of the same analysis techniques were used here to allow possible merging of the data and to facilitate comparison.

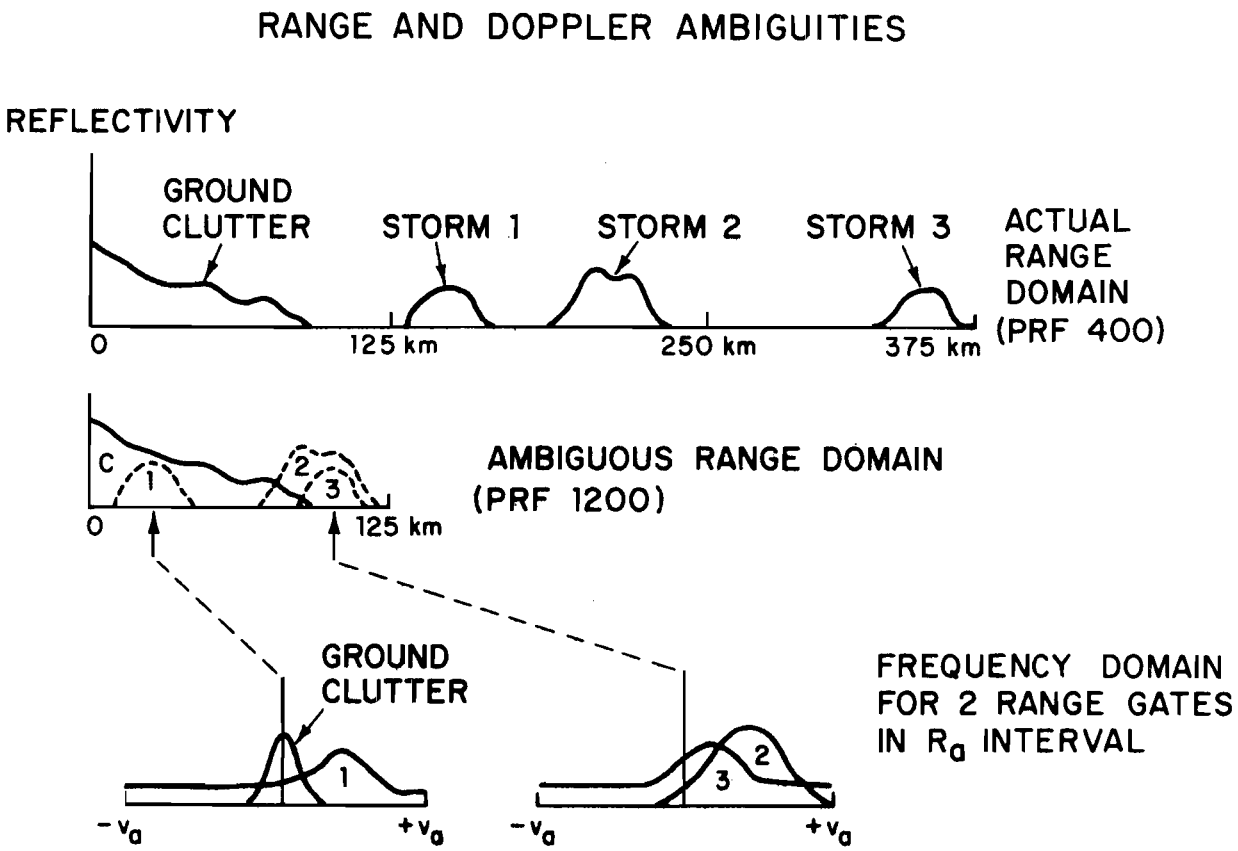

Fig. II-5. Storm geometry which leads to obscuration problems with conventional pulse Doppler radars. The overlap of weather signals can cause erroneous spectrum width and velocity estimates. (R_a is the unambiguous range.)

III. DISCUSSION OF TABLES

Data from the eight gust front cases are tabulated in Appendix A. The definition of each tabulated characteristic as well as any assumptions made in deriving the listed figures are presented in the following sections.

A. Height

The height of the gust front for each elevation angle was determined by locating the point on the outflow boundary which was most distant from the radar. At this point, either the beam was above the outflow, the outflow boundary was radially oriented and thus could not be detected, or the horizontal extent of the gust front had been reached. Data were collected for all scans in which the gust front was found. It was assumed that the height of the gust front for the maximum elevation at which it could be detected was indicative of the depth of the outflow. Table III-1 lists the maximum and minimum values of gust front height for each of the cases.

The average maximum height (depth) of the gust front is 2.5 km. This value is similar to the results of Zrnic' and Lee (1983, Z-L).

B. Length

The length of the gust front is the length of the line pattern (in either reflectivity, velocity or spectrum width displays) which could be identified as a gust front. Azimuth and range locations along the gust fronts were recorded and the lengths given in the tables are sums of the distances between these points. The greatest length recorded for the eight cases presented here was nearly 200 km, at the lowest elevation angle of the last scan on 2 May 1978. By this time the gust front had passed the radar and was dissipating. Comparing this maximum length to lengths observed by Z-L, one finds it to be at least twice as long. The minimum length was 6 km, noticeably less than the Z-L values.

Gust front length as detected by Doppler radar is highly variable. In general, gust front lengths appear to decrease at higher elevations. If an outflow has a fixed depth, as elevation angle increases a portion of the gust front will lie below the beam. Thus, the radar can only sense the nearer portions of the outflow and decreasing lengths at higher elevation angles are expected.

C. Doppler Velocities within the Outflow

Because it is impossible to display all possible values of reflectivity, velocity and spectrum width, these values are quantized when displayed. All values tabulated in Appendix A were derived from these displays. In the majority of the cases, exceeding the unambiguous velocity over a large area was rare, though velocities often fell into the highest interval. Cases in which large areas of velocity folding occurred were

TABLE III-1

MAXIMUM AND MINIMUM HEIGHTS (KM) FOR ALL GUST FRONTS

Date	Height (km) Max	Min
30 April 1978 (north)	3.7	2.5
30 April 1978 (south)	4.2	1.8
2 May 1978	1.1	0.3
19 June 1980	1.5	0.7
15 May 1982	2.7	0.9
30 May 1982	3.2	0.3
17 May 1983	2.3	0.4
10 June 1983	1.3	0.4
26 June 1984 (first)	3.6	0.3
26 June 1984 (second)	1.6	0.5
Average	2.5	0.8

30 May 1982 (an apparent downburst situation) and 17 May 1982 (a bow echo case). The maximum radial wind speed measured for all eight cases was $-43\ ms^{-1}$ on 17 May 1982.

D. Reflectivity along the Gust Front

The value of peak reflectivity varied from a low of 7 dBZ, which agrees with the Z-L findings, to a maximum value exceeding 57 dBZ. The peak reflectivity for the majority of scans was greater than 30 dBZ. In many cases the gust front either did not separate from the precipitation echo or did separate to form a thin line echo but remained attached to the parent storm. In these cases, the maximum reflectivities recorded represent precipitation returns. Also, convection occurring along the outflow boundary could produce the high reflectivity values listed in the table.

E. Spectrum Width

As stated previously, the turbulence that occurs along the gust front can be sensed by Doppler radar and often appears as a linear pattern in the spectrum width field. The maximum and minimum values in Appendix A are often associated with small areas scattered along the outflow boundary. Thus, the more meaningful statistic is probably the average spectrum width. This value tends to decrease with increasing elevation angle, suggesting (not surprisingly) that turbulence is greater near the surface.

The significance of the average spectrum width in the gust front is not its absolute value but how it compares to the surroundings. Gust fronts can appear as lines of enhanced turbulence in a relatively quiescent field.

F. Distance from Gust Front to Generating Storm

This value represents the shortest distance between the center of the parent storm and the leading edge of the outflow. The center of the generating storm is assumed to be associated with the area of maximum reflectivity within the parent cell. The distance between the generating storm and gust front is expected to decrease with height. (Refer to Fig. II-2.) Near the surface, the boundary between the cold air outflow and warm environmental air is far from the storm. This boundary slopes back toward (closer to) the parent cell with increasing height. As the gust front moves away from the storm, the distance between the generating storm and the outflow boundary increases.

The values in Appendix A generally support these statements. It is important to note, however, that as a storm cell evolves, the area of maximum reflectivity within the cell moves in response to the formation of updrafts and downdrafts. This may account for any discrepancies in the tabulated values.

G. Radial Shear

Appendix B lists radial velocities and radial shears for three gust fronts. The shear values were obtained by the use of a radial convergence detection algorithm presently being developed and tested at NSSL (Zrnic' and Uyeda, 1984). The algorithm searches each radial for runs of decreasing velocities. It stores the beginning and ending range and velocities for each run and uses these to calculate radial shear. A low shear threshold can be specified below which the radial shear is considered insufficient to be part of the gust front. This threshold was chosen to be 0.50 ms^{-1} km^{-1} (0.50 x 10^{-3} s^{-1}). Since this algorithm uses the entire length of the convergence along a radial to calculate shear, it may tend to smooth very high shears that occur at the leading edge. It should be noted that the values in Appendix B represent radial shear only. No attempt was made to relate Doppler radial shear to actual shear in the total wind field.

The maximum radial shear for the three gust fronts presented in Appendix B is 12.39 x 10^{-3} s^{-1} on 30 May 1982. As expected, the largest shears were found where the outflow boundary was perpendicular to the beam (i.e., flow behind the boundary had a strong radial component). Lower shears were located at the ends of the gust fronts where curvature caused the boundary to lie along a radial. In some of these cases, even though the gust front was identifiable in the displays, radial shear values did not exceed the threshold. In general both minimum and maximum values of radial shear increase with height and the greatest radial shears are associated with the greatest velocities.

IV. CASE STUDIES

A. Case 1: 30 April 1978

1. Synoptic Situation

A stationary front oriented northeast-southwest across Oklahoma and an approaching upper air disturbance provided the impetus for an outbreak of severe weather in Texas, Oklahoma and Kansas. Storms formed along and north of the front. By 1900 CST, a line of storms, approximately 40 km long and 80 km southwest of Oklahoma City (OKC), developed and moved east-northeast. At 2030 CST two lines of radial shear (radial convergence) were evident in the Doppler wind field, indicating the presence of gust fronts. The northern gust front was associated with a cell at an azimuth of 281° and range of 56 km (i.e., 281°/56 km) and the southern gust front with a cell at 261°/66 km. (Henceforth, all azimuth and range coordinates will be given in this notation.)

2. Doppler Radar Displays

Photographs* of the three spectral moments are displayed in Figures IV-1(a) through IV-1(c). In the reflectivity field (Fig. IV-1(a)), the gust fronts (labels A and B) appear as lines of enhanced reflectivity which have separated from and lie 3-5 km ahead of the leading edge of the precipitation echo. In this photo, and in the majority of the subsequent photos, 10 dBZ was added in order to ensure that the signal was brought above a threshold level. Therefore, although the peak reflectivity in the gust front appears to be 21 dBZ, it is actually 11 dBZ.

The location of the gust front in the velocity display (Fig. IV-1(b)) is indicated by the zero velocity contour (label C) at its leading edge. The most well-defined outflow boundary occurs where the radial component of the outflow winds is maximized (e.g., 240°/30 km; label D). Notice the southerly environmental winds in the region east of the gust front. The winds immediately ahead of the gust front are stronger than the environmental winds elsewhere in the field. Based upon the observed evolution of the Doppler wind field, these winds are accelerating, presumably in response to the intrusion of the cold air outflow into the environmental flow.

This case also illustrates the ability of Doppler radar to detect a gust front when it lies along a radial. The winds associated with the northern gust front (label E) and with the southern extension of the southern gust front (label D) are primarily directed across the radar beam.

---

* For interpretation of the displays shown in these photographs, refer to Appendix C.

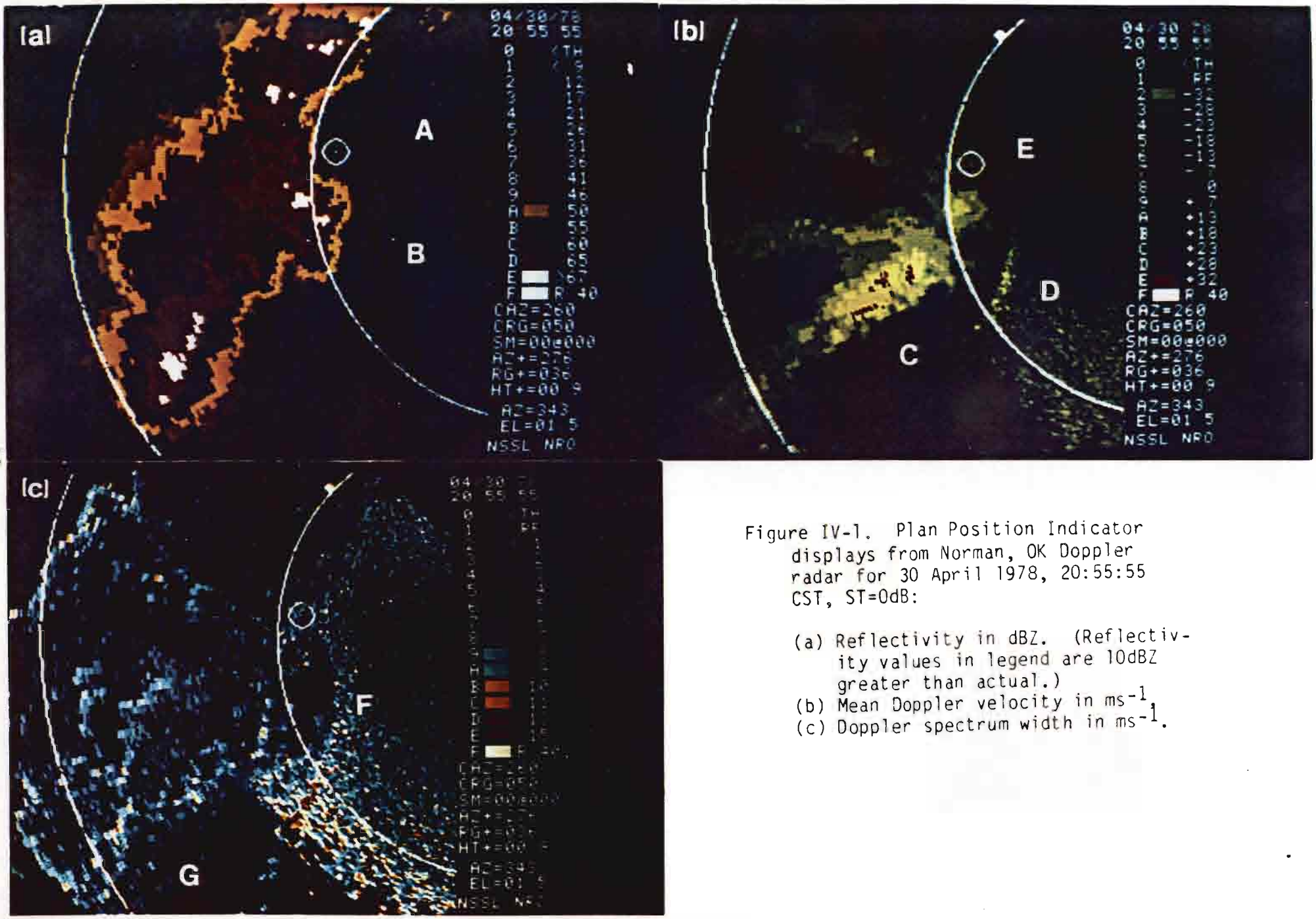

Figure IV-1. Plan Position Indicator displays from Norman, OK Doppler radar for 30 April 1978, 20:55:55 CST, ST=0dB:

(a) Reflectivity in dBZ. (Reflectivity values in legend are 10dBZ greater than actual.)
(b) Mean Doppler velocity in ms^{-1},
(c) Doppler spectrum width in ms^{-1}.

Hence, the boundary between environmental and outflow winds is not well-defined. (An example of this is the broadening of the zero velocity contour near label C.) In these areas the gust fronts are associated with azimuthal shearing of the radial winds.

Figure IV-1(c) is a display of the velocity spectrum width (ms^{-1}). A gust front will often appear as a linear pattern of enhanced spectrum width which closely parallels the gust front signature in the velocity field. In this case, the location of the gust front is indicated by the sharp division between the larger spectrum widths in the environmental flow (low signal-to-noise ratio) and the lower values in the outflow (label F). However, as the gust front becomes radially oriented, the spectrum width pattern disappears (label G). This result is somewhat unexpected. It is assumed that turbulence is isotropic (i.e., exhibits the same value when measured along any axis). If this were true, the line of enhanced spectrum widths would be present near label G. Either the assumption is invalid in this case or this area simply is not turbulent.

As the storms moved to the northeast, the southern cell intensified and the northern gust front dissipated. The gust fronts propagated at a speed of 11 ms^{-1}. Figures IV-1(d) through IV-1(f) show the radar displays at 2217 CST. The linear feature indicated by the cursor is the southern end of the southern gust front. The northern portion has moved into an area of range folding (that is, the first trip return is not 10 dB greater than the second trip return; label H). At this time, the gust front has moved away from the generating storm, creating a thin line echo with a peak reflectivity of 11 dBZ (the 21 dBZ category). The spectrum widths increase dramatically at the edges of echoes (label I) and near areas of range folding (label J). Within the outflow (cursor) the spectrum width decreases, probably due to the higher SNR in this region.

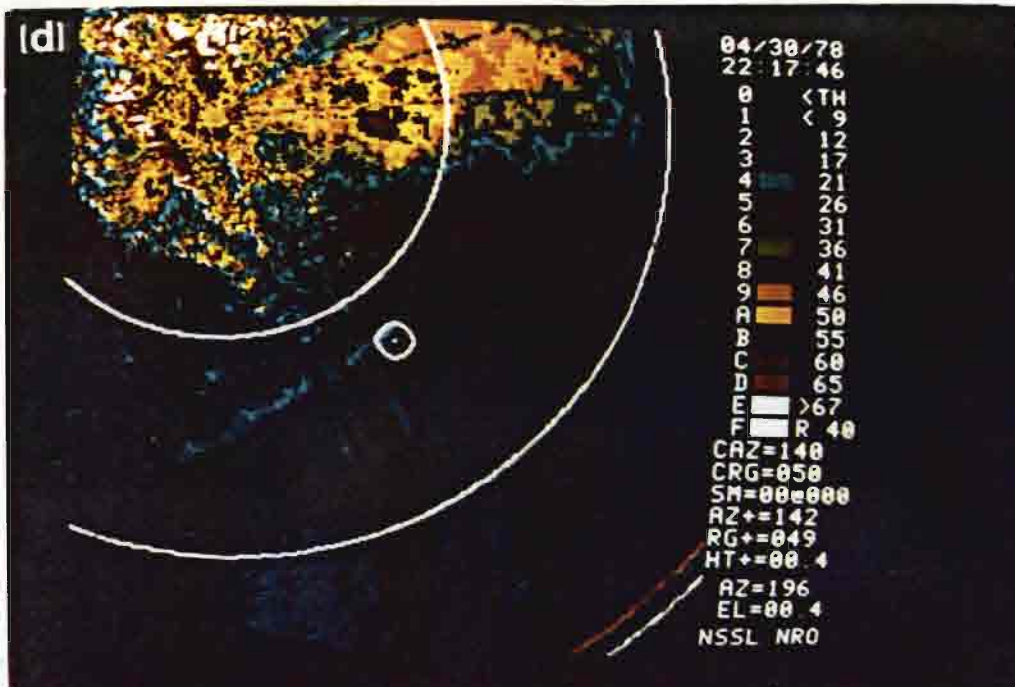

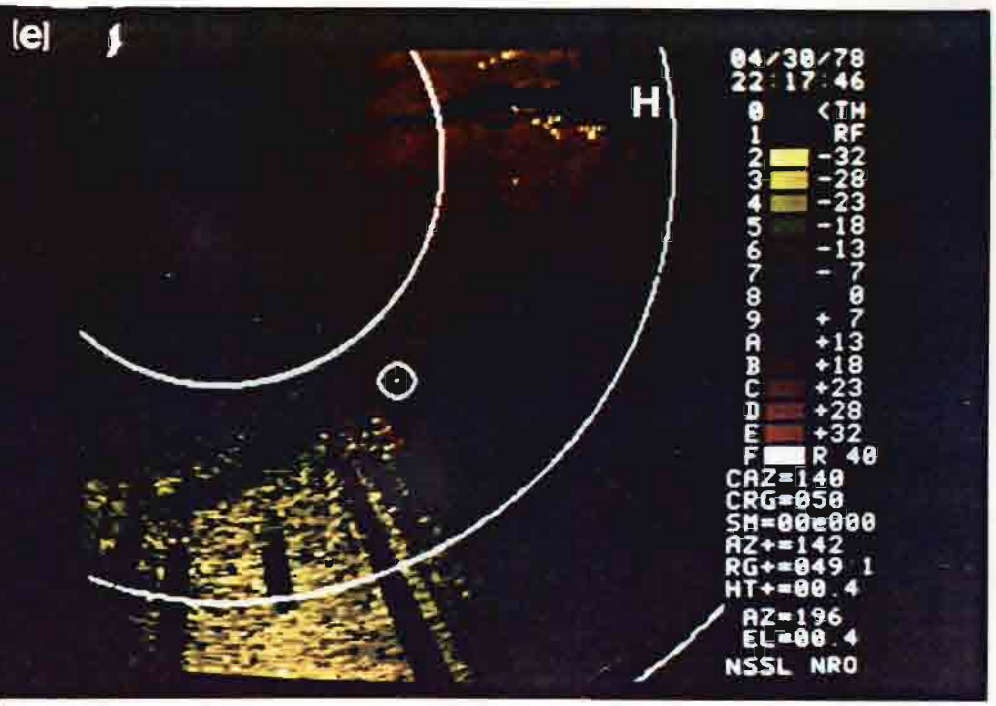

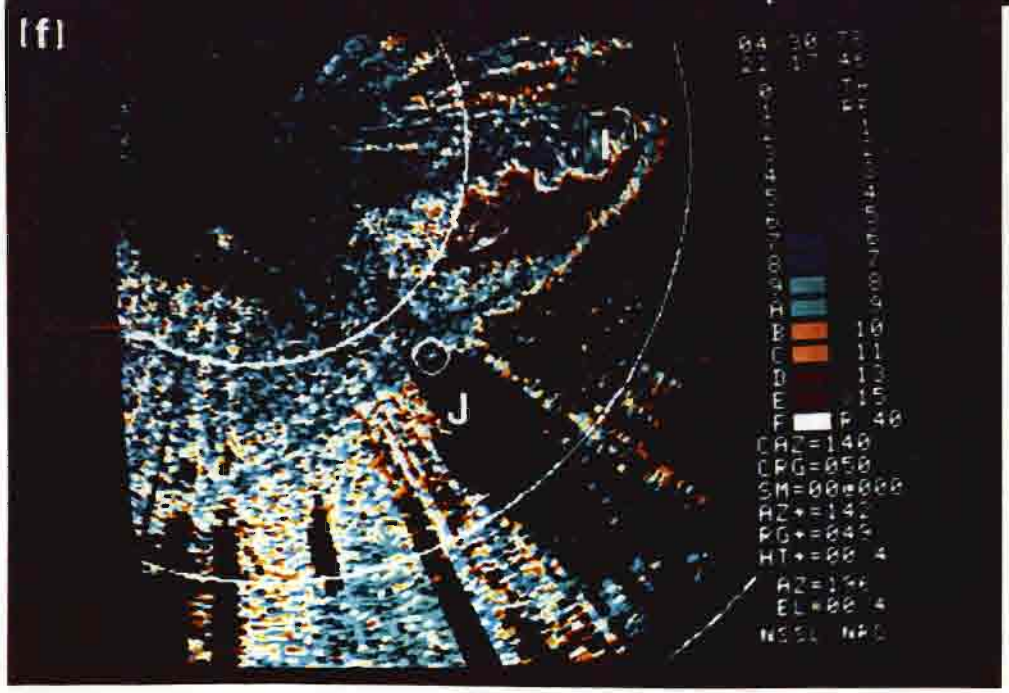

(d) Same as (a), except at 22:17:46 CST.
(e) Same as (b), except at 22:17:46 CST.
(f) Same as (c), except at 22:17:46 CST.

B. Case 2: 2 May 1978

1. Doppler Radar Displays

This gust front occurred ahead of a line of strong thunderstorms oriented northwest to southeast. The outflow moved to the northeast at about 17 ms^{-1}. Figures IV-2(a) through IV-2(c) show the reflectivity, velocity and spectrum width fields associated with this gust front. There is no thin line echo in the reflectivity field (Fig. IV-2(a)) to indicate the presence of the outflow. Throughout its lifetime, the gust front never moved far enough away from the storm to form the thin line signature. There is also no obvious pattern in the spectrum width field (Fig. IV-2(c)).

In this case, the gust front can only be detected in the Doppler velocity field (Fig. IV-2(b)). The change in wind direction at the leading edge of the outflow (label A) is quite pronounced. An interesting feature on the velocity display is the banded structure of the outflow. There are 4 or 5 lines of radial wind minima parallel to the outflow leading edge (label B) and separated by about 10 km. It is believed that these are secondary surges, which are disturbances in the outflow parallel to but behind the gust front. Secondary surges were first identified by Goff (1975) in data collected by the instrumented WKY-TV tower. By plotting these data versus time, the disturbances can be readily identified. Secondary surges often exhibit characteristics associated with the passage of a gust front (i.e., abrupt changes in wind speed and direction, temperature drop, etc.). There has also been evidence of secondary surges in mesonet data (Charba, 1972). Little is known about these disturbances, beyond the fact that they exist. It is currently assumed that they do not affect the character (propagation and structure) of the leading edge of the outflow, but there is little evidence to support this assumption at present. It is sufficient to note here that the banded structure (label B) in the outflow maintained its structure as the outflow propagated to the northeast.

2. Tower Data

Figure IV-2(d) shows data gathered at the WKY-TV tower during the passage of the gust front. In these plots time increases to the left, producing an approximate spatial representation of the gust front. The outflow boundary (1815 CST) is marked by an abrupt wind direction change and rising motion in the streamlines, a slight cooling in the potential temperature field and an increase in the component of the wind perpendicular to the boundary. There is no evidence of a gust front in the vertical velocity and parallel wind component plots. There is a disturbance in the streamline analysis at 1827 CST, located approximately 10 km behind the leading edge of the outflow, which corresponds to the banding in the Doppler velocity field. The streamline pattern at 1825 CST indicates the

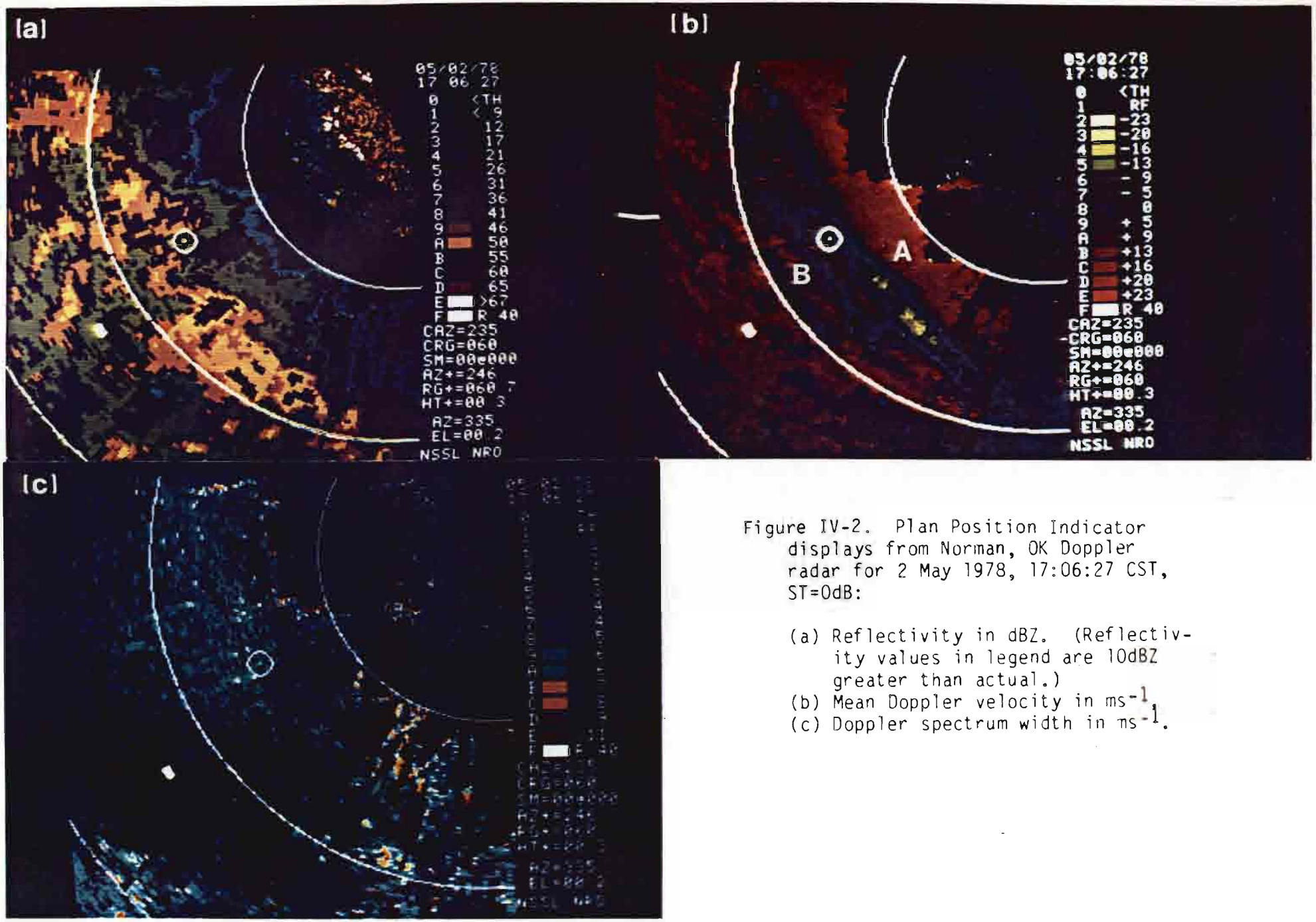

Figure IV-2. Plan Position Indicator displays from Norman, OK Doppler radar for 2 May 1978, 17:06:27 CST, ST=0dB:

(a) Reflectivity in dBZ. (Reflectivity values in legend are 10dBZ greater than actual.)
(b) Mean Doppler velocity in ms^{-1},
(c) Doppler spectrum width in ms^{-1}.

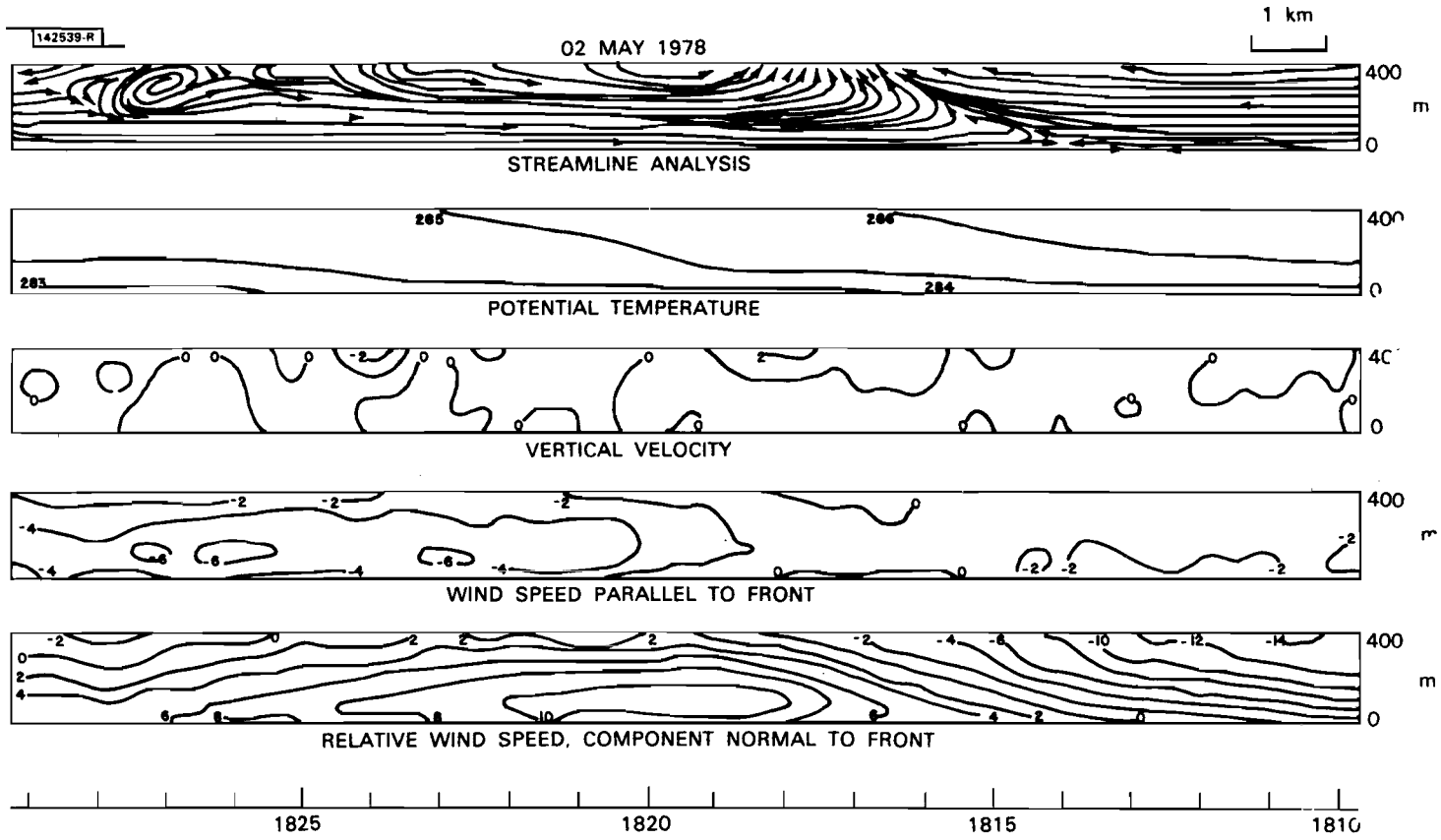

Fig. IV-2(d). Plots of WKY-TV tower data collected during the passage of the gust front (1810-1829 CST) on 2 May 1978.

location of the storm's downdraft. Thus, the aforementioned disturbance is within the outflow moving toward the rear of the storm. Subsequent disturbances are found in the tower data not shown here. This tends to substantiate the presence of secondary surges inferred from the single Doppler data.

C. Case 3: 19 June 1980

1. Synoptic Situation

A surface warm front across southern and central Texas and an upper level short wave trough combined to produce severe thunderstorms. The storm that generated the gust front in this case study developed around 2130 CST and moved east-southeast. However neither the storm nor the gust front were scanned by Doppler radar until about 2215 CST.

2. Doppler Radar Display

The first scan taken was a full PPI which showed that the gust front stretched from 270° to 360° at a distance of about 40 km (see Fig. IV-3(a) through IV-3(c)). In Fig. IV-3(a), the cursor indicates a portion of the gust front that separated from the precipitation echo to form a thin line (320°/35 km). However, the pattern in the velocity field (Fig. IV-3(c)) suggests that the southern portion of the gust front (label A) is not associated with a thin line echo (label B) in Figure IV-3(a). There is no definite pattern in the spectrum width field to indicate the presence of the gust front. The area of enhanced spectrum widths at label C is in clear air, which implies a weak signal. Although the signal is strong enough to allow detection of the outflow (label A, Fig. IV-3(b)) in the mean velocity field, weak signals produce invalid spectrum width estimates which cause the display to appear very "noisy". The signal-to-noise ratio threshold (ST) in Figure IV-3(c) is 0 dB. Increasing the threshold to 10 dB (Fig. IV-3(d)) removes all information in this area (label D).

3. Tower Data

After completion of a volume scan at full PPI, the radar began sector scanning the storm at position E (Fig. IV-3(a)). Hence, only a portion of the gust front was scanned. The outflow moved south-southeast at 10 ms^{-1} and crossed the tower at 2213 CST. Figure IV-3(e) shows the plots of the tower data. The passage of the leading edge of the outflow produced a nearly indiscernible cooling in the potential temperature field and a gradual but noticeable increase in the component of the wind perpendicular to the gust front.

4. Thermodynamic Sounding

Figure IV-3(f) is the sounding from Norman (OUN), OK which was taken approximately one hour before the arrival of the storm. This sounding is characterized by strong directional shear from 950 mb to 750 mb, but little speed shear. A slight inversion is present at 1 km. The lifted index is approximately -7.

Fig. IV-3. Plan Position Indicator displays from Norman, OK Doppler radar for 19 June 1980, 22:18:44 CST:

(a) Reflectivity in dBZ.
(b) Mean Doppler velocity in ms^{-1}.
(c) Doppler spectrum width in ms^{-1}.
(d) Same as (c), except at 22:18:40 CST, ST=10 dB.

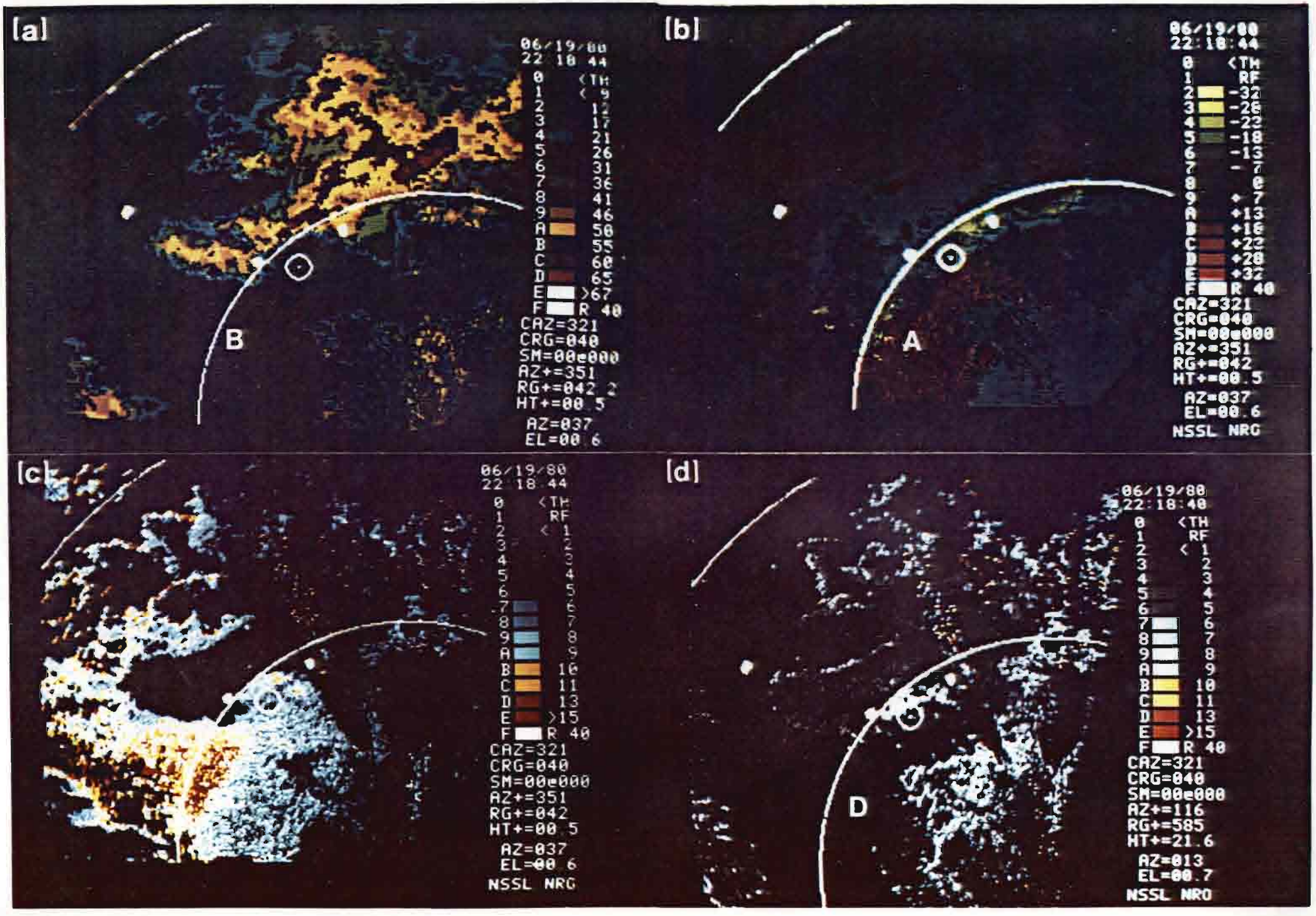
[a]
06/19/80
22 18 44
0 <TH
1 < 9
2 12
3 17
4 21
5 26
6 31
7 36
8 41
9 46
A 50
B 55
C 60
D 65
E >67
F R 40
CAZ=321
CRG=040
SM=00e000
AZ+=351
RG+=042 2
HT+=00 5
AZ=037
EL=00 6
B
[b]
06/19/80
22:18:44
0 <TH
1 RF
2 -32
3 -28
4 -23
5 -18
6 -13
7 - 7
8 0 7
9 +13
A +16
B +22
C +28
D +32
E
F R 40
CAZ=321
CRG=040
SM=00e000
AZ+=351
RG+=042
HT+=00.5
AZ=037
EL=00.6
NSSL NRG
A
[c]
06/19/80
22 18 44
0 <TH
1 RF
2 < 1
3 2
4 3
5 4
6 5
7 6
8 7
9 8
A 9
B 10
C 11
D 13
E >15
F R 40
CAZ=321
CRG=040
SM=00e000
AZ+=351
RG+=042
HT+=00 5
AZ=037
EL=00 6
NSSL NRG
[d]
06/19/80
22:18:40
0 <TH
1 RF
2 < 1
3 2
4 3
5 4
6 5
7 6
8 7
9 8
A 9
B 10
C 11
D 13
E >15
F R 40
CAZ=321
CRG=040
SM=00e000
AZ+=116
RG+=585
HT+=21.6
AZ=013
EL=00.7
NSSL NRO
D

Fig. IV-3.

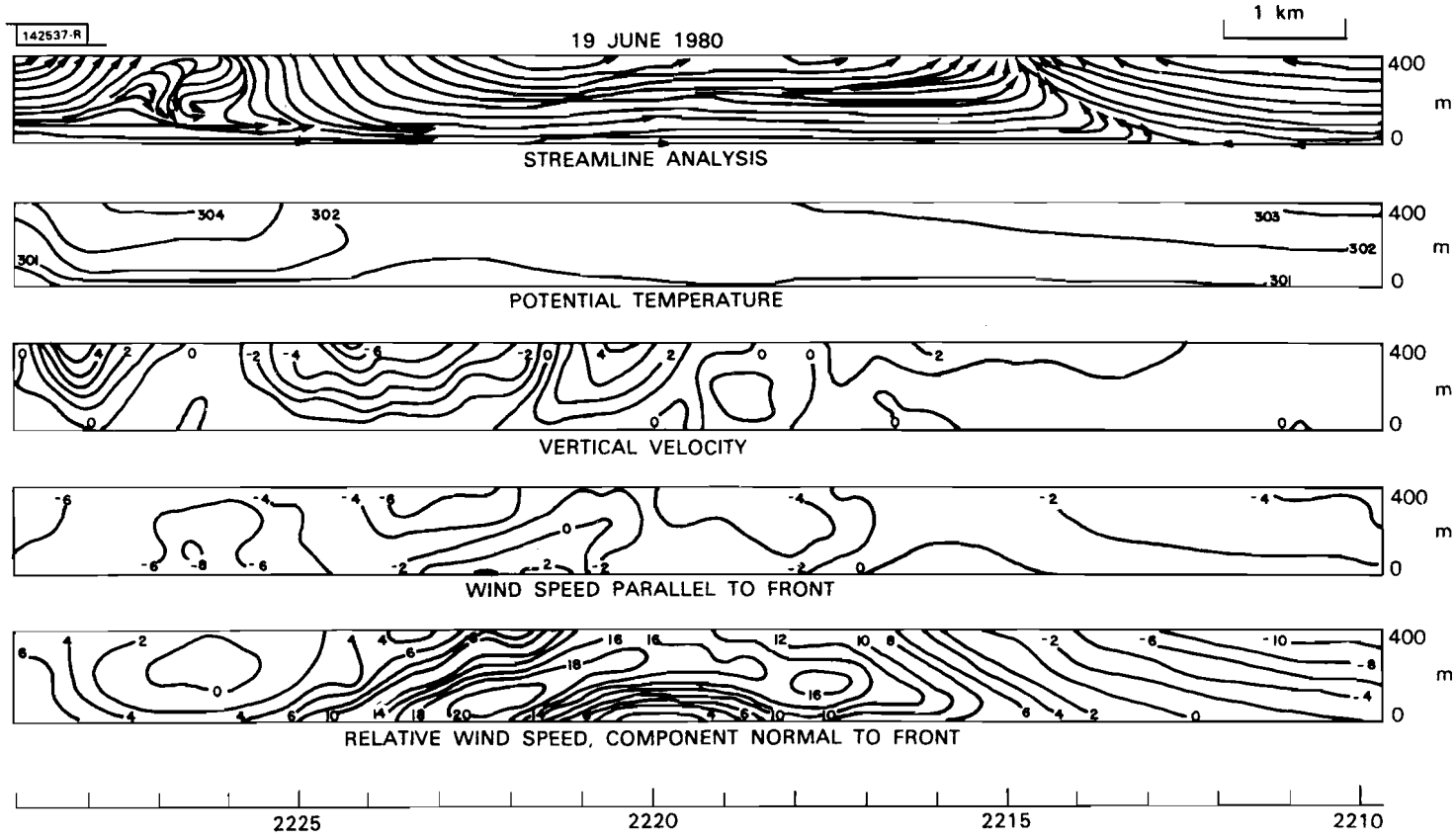

Fig. IV-3(e). Plots of WKY-TV tower data collected during the passage of the gust front (2210-2229 CST) on 19 June 1980.

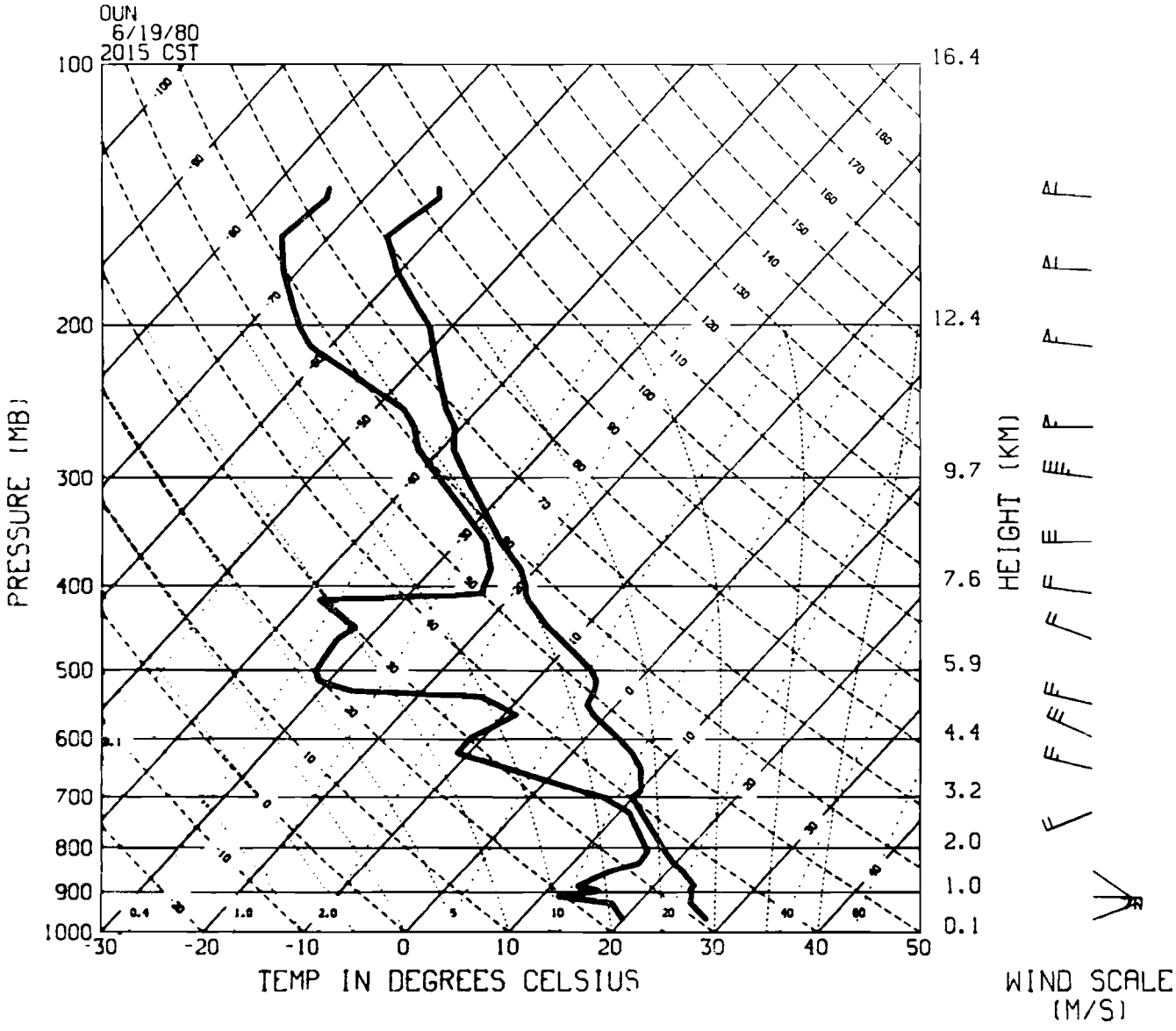

Fig. IV-3(f). Thermodynamic sounding taken at Norman (OUN), OK at 2015 CST 19 June 1980.

D. Case 4: 15 May 1982

1. Doppler Radar Displays

This gust front was produced by a cell that developed 80 km west of Norman, OK (NRO) and propagated eastward. The Doppler radar began scanning this storm at approximately 1930 CST, after the gust front had already begun to develop. Figures IV-4(a) through IV-4(c) show the Doppler displays for 20:14:18 CST. The gust front has separated from the parent storm (Fig. IV-4(a)) and formed a thin line signature (cursor). The velocity field (Fig. IV-4(b)) shows inbound velocities coincident with the thin line (cursor) and outbound velocities on either side. The outbound velocities occur in clear air and the spectrum widths in Fig. IV-4(c) are correspondingly large (label A). Some range folding is apparent in Fig. IV-4(b) (label B). As in Case 1, spectrum width (Fig. IV-4(c)) increased near range folded regions (label C). Although the pattern is not obvious, there is some enhancement in the spectrum width field that is associated with the outflow (label D).

2. Tower Data

Plots of the tower data are given in Fig. IV-4(d). The streamline plot shows convergence occurring at a level of 300 m in the environmental air. The gust front reached the tower at 2037 CST, which is indicated by the rapid cooling in the potential temperature field and increases in all three wind speed components.

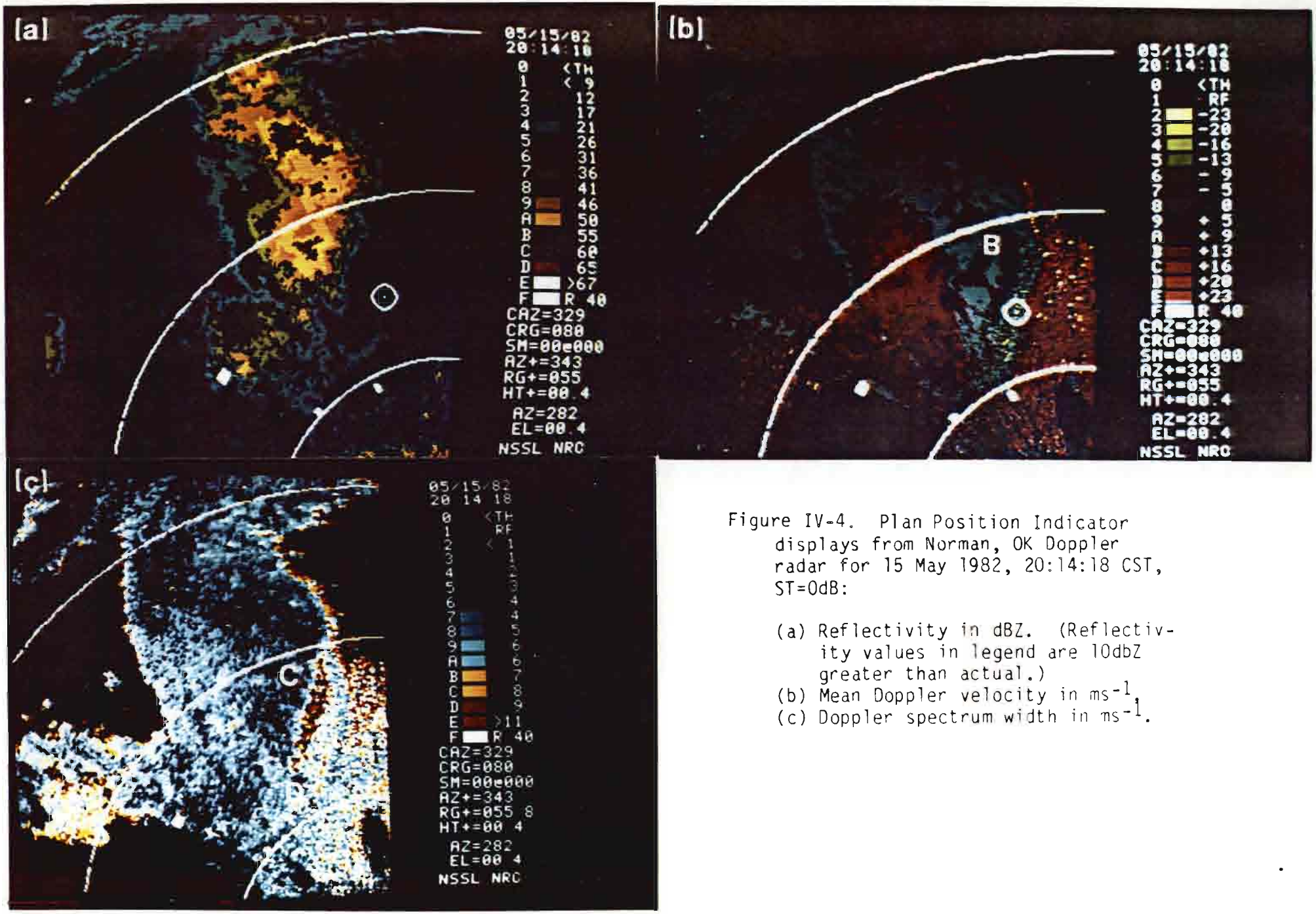

Figure IV-4. Plan Position Indicator displays from Norman, OK Doppler radar for 15 May 1982, 20:14:18 CST, ST=0dB:

(a) Reflectivity in dBZ. (Reflectivity values in legend are 10dbZ greater than actual.)
(b) Mean Doppler velocity in ms^{-1},
(c) Doppler spectrum width in ms^{-1}.

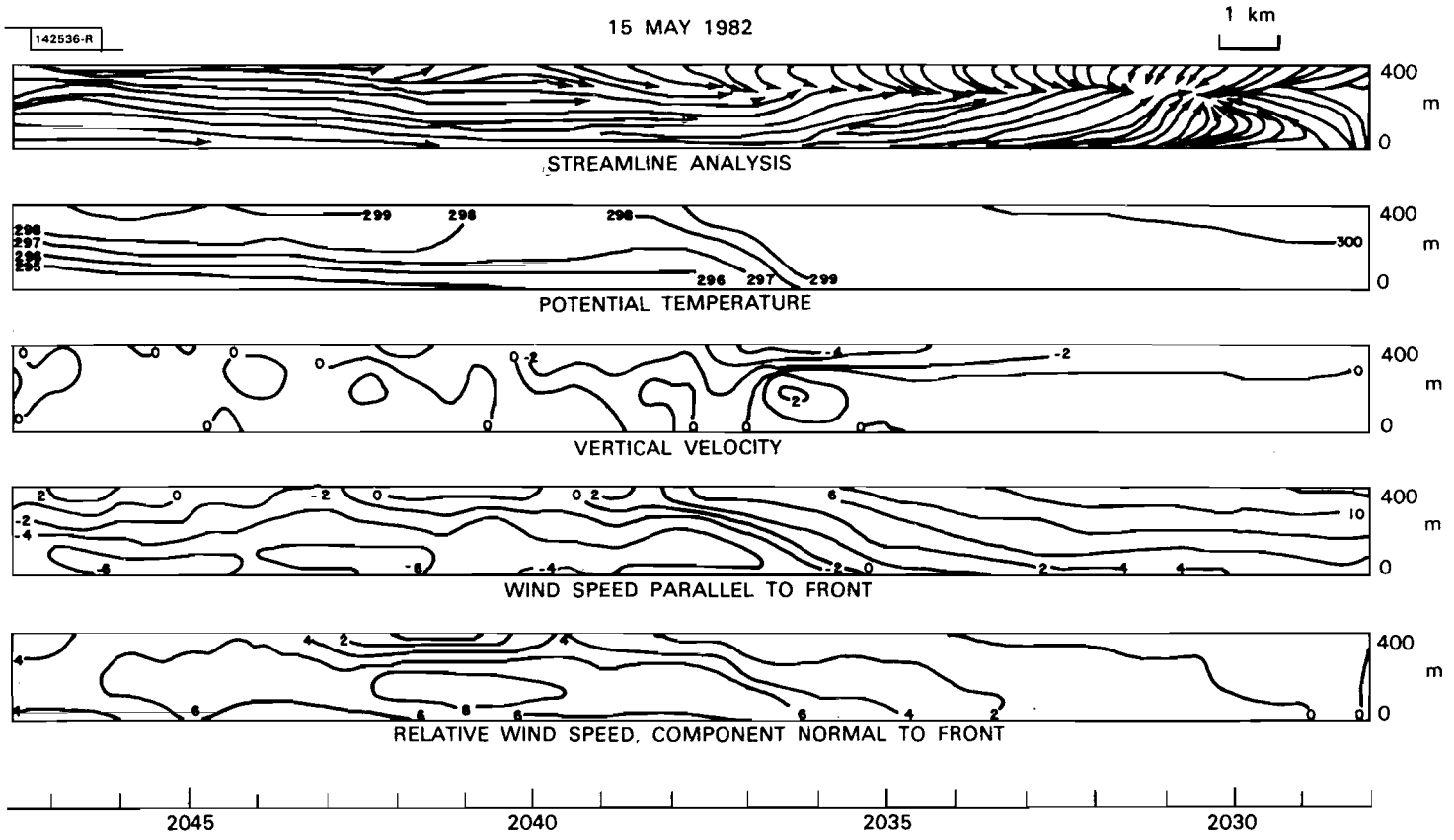

Fig. IV-4(d). Plots of the WKY-TV tower data collected during the passage of the gust front (2028-2047 CST) on 15 May 1982.

E. Case 5: 30 May 1982

1. Synoptic Situation

On this day, a surface low pressure center was located in north-central Oklahoma with an associated frontal system oriented east-west across extreme northern Oklahoma. A dryline extended south-southwest along the Texas-Oklahoma border and a surface low pressure trough stretched from north-central Oklahoma into central Texas. Thunderstorms developed in western Oklahoma as the dryline moved eastward.

2. Doppler Radar Displays

The gust front is depicted in the three spectral moment displays presented in Figures IV-5(a) through IV-5(c). The cursor marks the interface between the outflow and environmental air (Fig. IV-5(b)). The gust front has not moved away from the storm to form a thin line echo (Fig. IV-5(a)). However, contrary to most of the previous cases, a well-defined linear pattern of enhanced spectrum width (Fig. IV-5(c)) is present at the outflow edge (cursor).

The large area of folded velocities (35 ms^{-1}, label A) in Fig. IV-5(b) is a feature of interest. Dual Doppler data is available for this time and is presently being analyzed at NSSL. Preliminary results indicate the presence of one or more downbursts in this region (Eilts, personal communication). The bulge of the gust front (label B, Fig. IV-5(b)) in this display may be a bow echo, which has been identified as a possible characteristic of downbursts (Fujita, 1981).

Figures IV-5(d) through IV-5(f) show the same gust front at a later time. The outflow boundary has propagated eastward at about 20 ms^{-1}. The wave located near the cursor in Fig. IV-5(b) has disappeared (Fig. IV-5(e)) and a larger portion of the flow has become perpendicular to the radar beam (the area of zero velocity is larger than in Fig. IV-5(b)). The leading edge of the outflow has moved ahead of the precipitation but does not appear to have an associated echo line. Identification of the thin line may be hampered by ground clutter in the area. Fig. IV-5(e) indicates that relative to the environmental flow, the outflow is more turbulent (label C) and the division between the two flows is still pronounced (cursor).

3. Tower Data

Presented in Fig. IV-5(g) are plots of the WKY-TV tower data. The gust front reached the tower at 2115 CST, as can be seen most dramatically in the potential temperature field. The passage of this gust front is also accompanied by marked changes in all three wind components (2116 CST) and the transition from turbulent flow ahead to roughly laminar flow behind the outflow boundary.

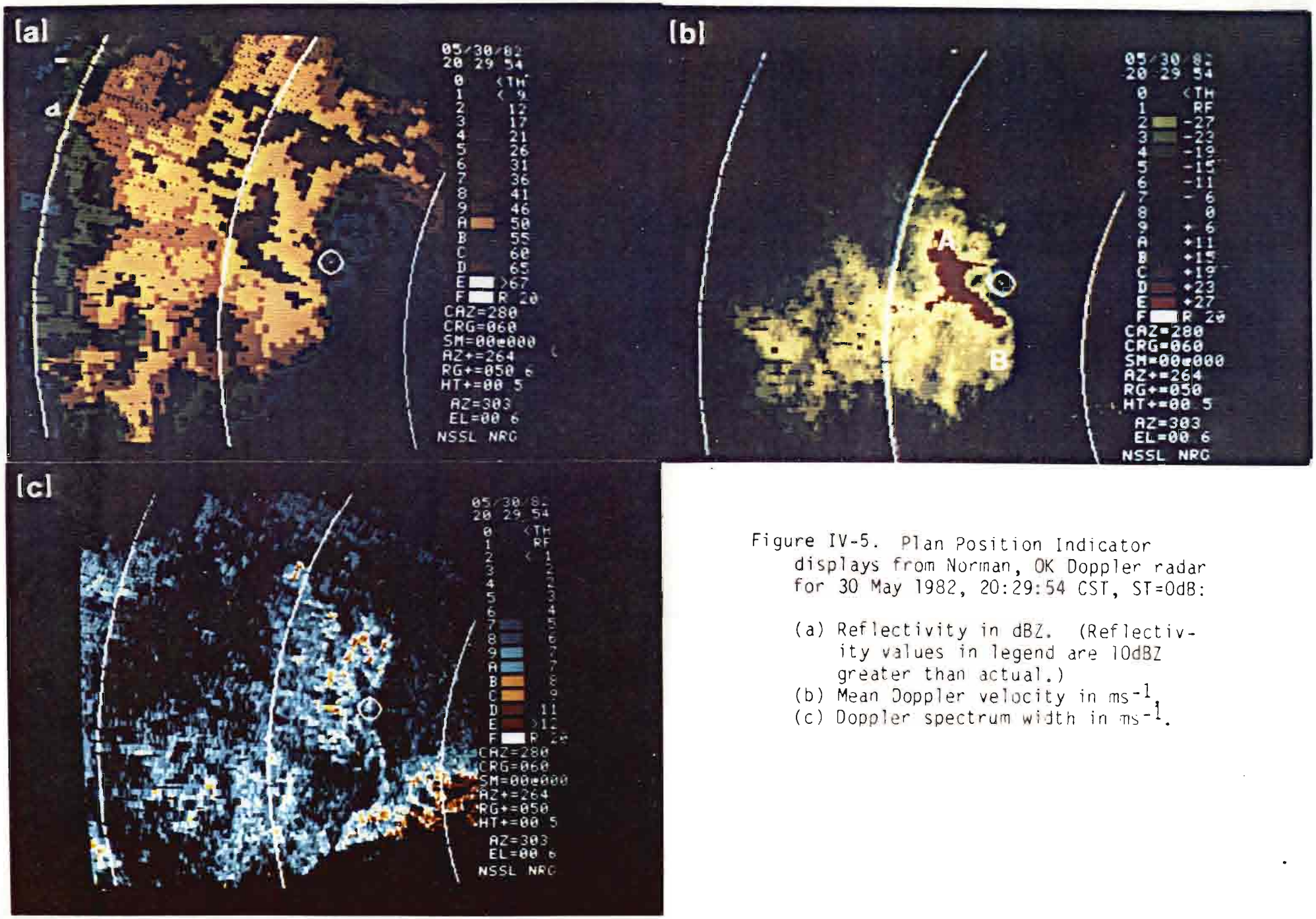

Figure IV-5. Plan Position Indicator displays from Norman, OK Doppler radar for 30 May 1982, 20:29:54 CST, ST=0dB:

(a) Reflectivity in dBZ. (Reflectivity values in legend are 10dBZ greater than actual.)
(b) Mean Doppler velocity in ms^{-1},
(c) Doppler spectrum width in ms^{-1}.

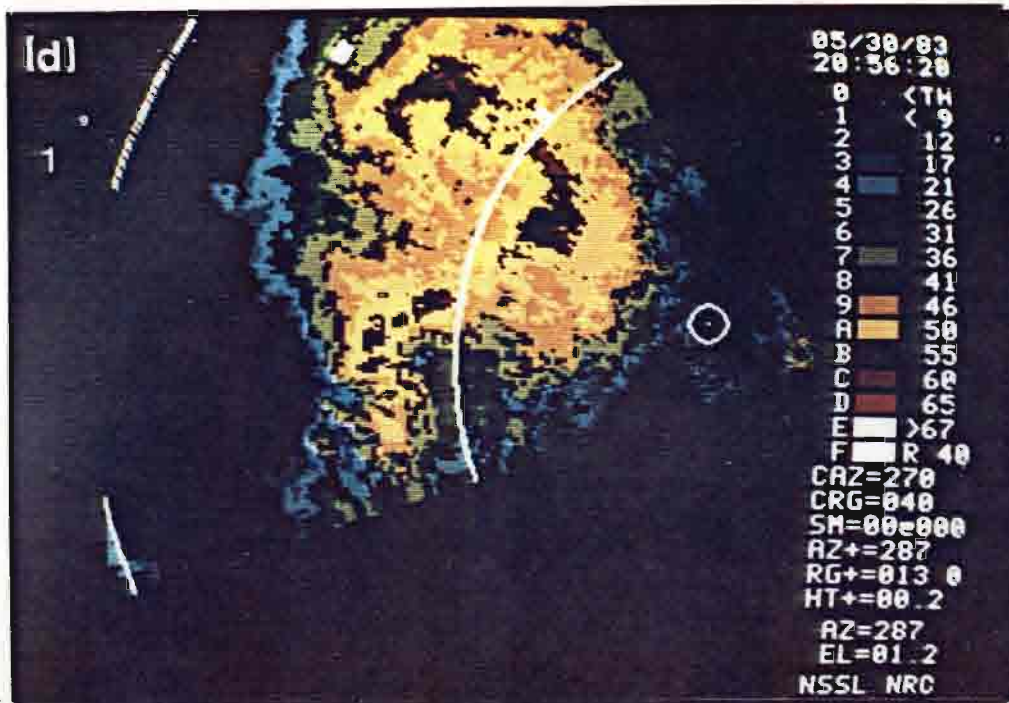

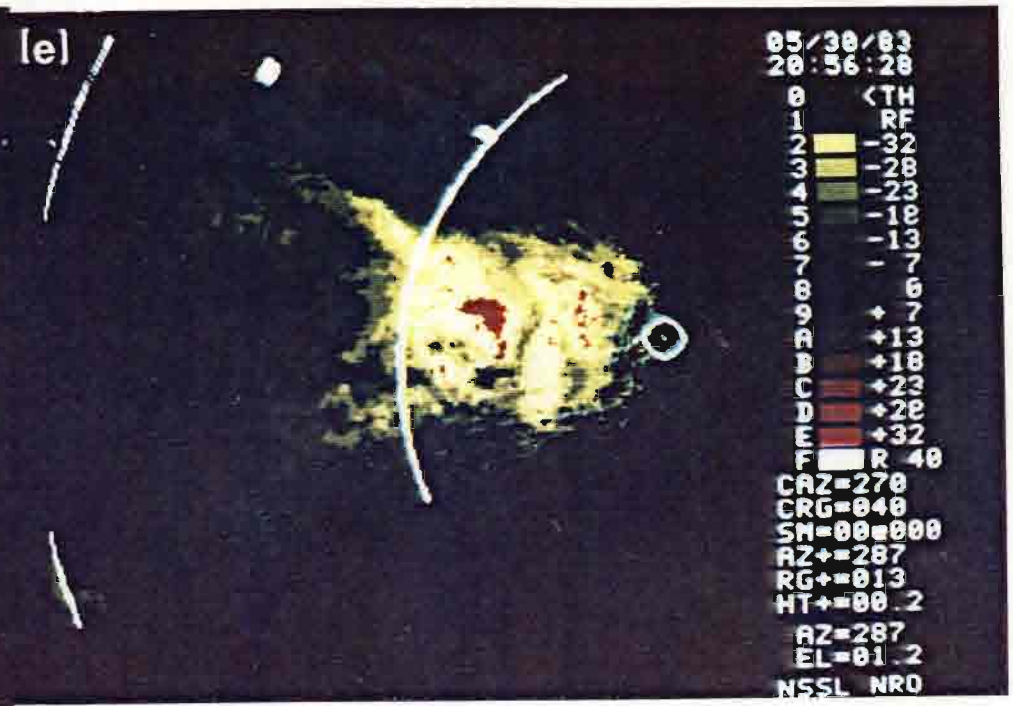

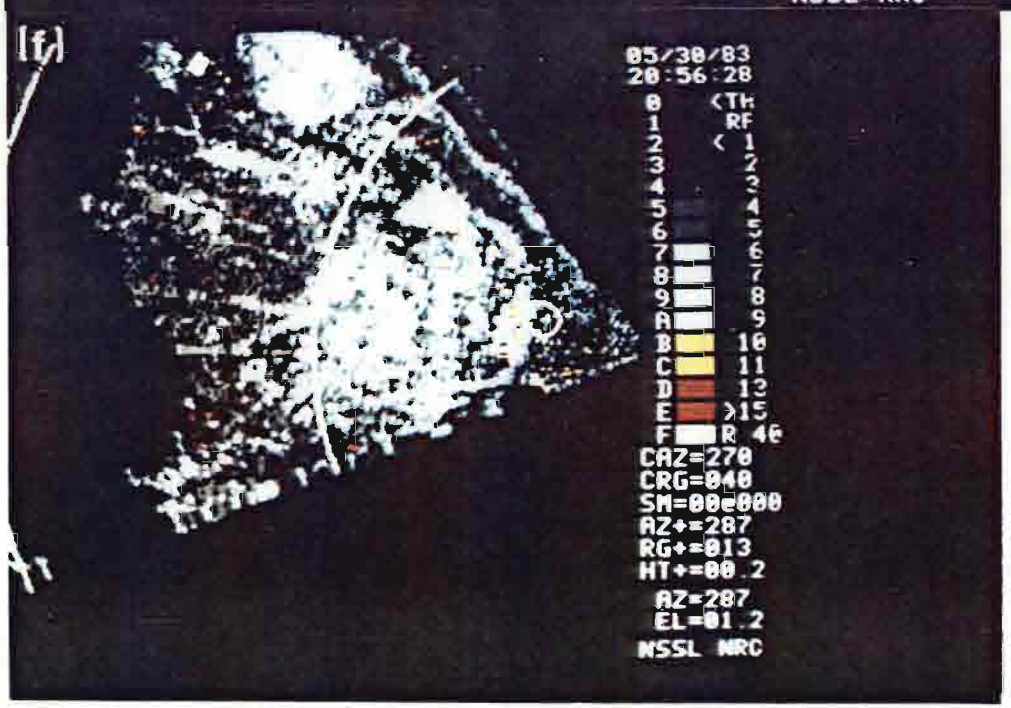

(d) Same as (a), except for 20:56:28 CST (Note: year is 1982 not 1983).
(e) Same as (b), except for 20:56:28 CST.
(f) Same as (c), except for 20:56:28 CST.

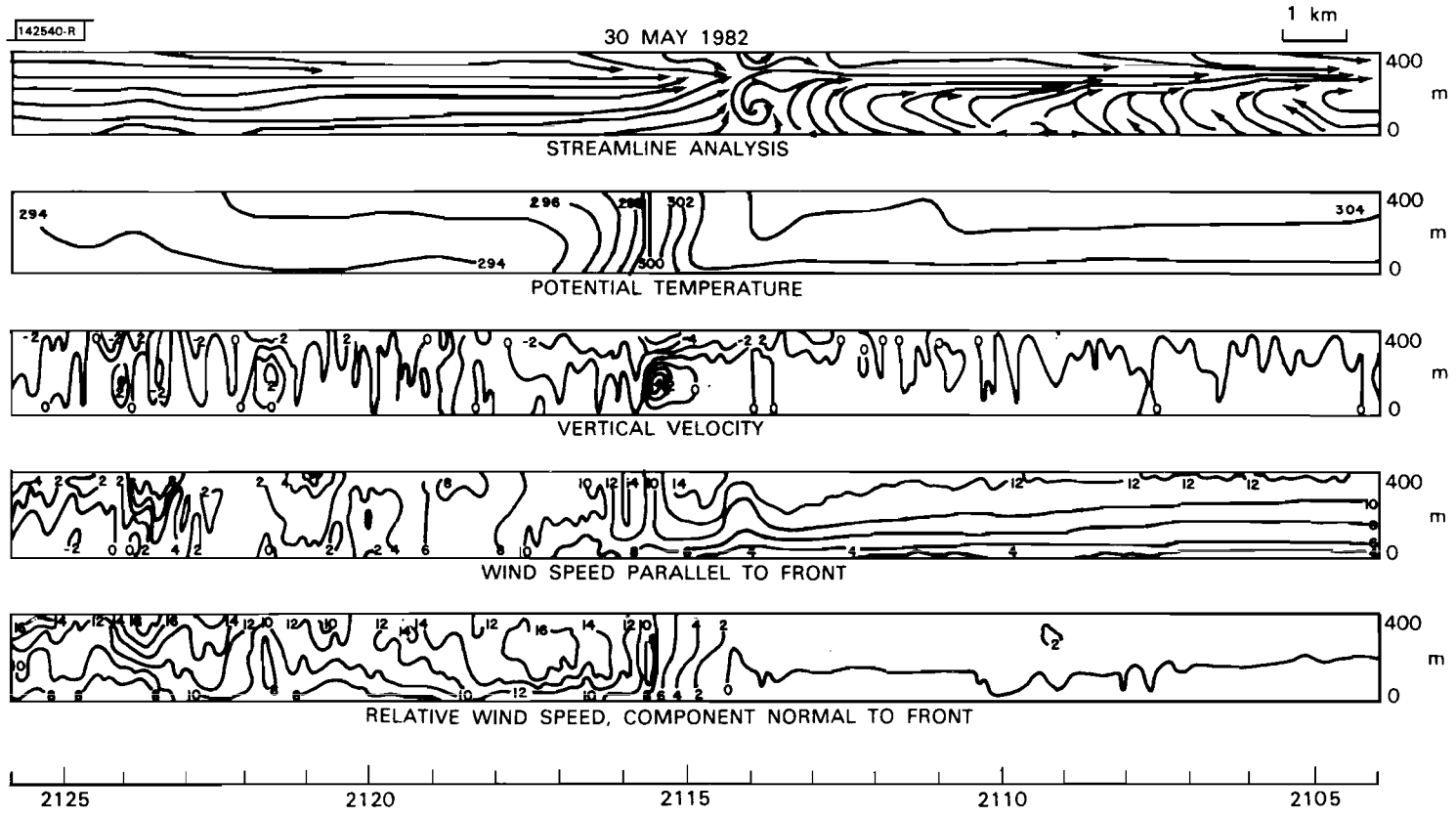

Fig. IV-5(g). Plots of the WKY-TV tower data collected during the passage of the gust front (2104-2125 CST) on 30 May 1982.

4. Thermodynamic Sounding

Figure IV-5(h) is the sounding taken at Tuttle (TTS), OK at 1900 CST, about one hour prior to the arrival of the thunderstorms. The veering of the winds with height is dynamically significant for the formation of severe thunderstorms (Klemp and Wilhelmson, 1978). The atmosphere is quite moist below 800 mb and dry above. The lifted index for this sounding is roughly -11 (an extremely unstable atmosphere) with very little capping from the 800 mb inversion.

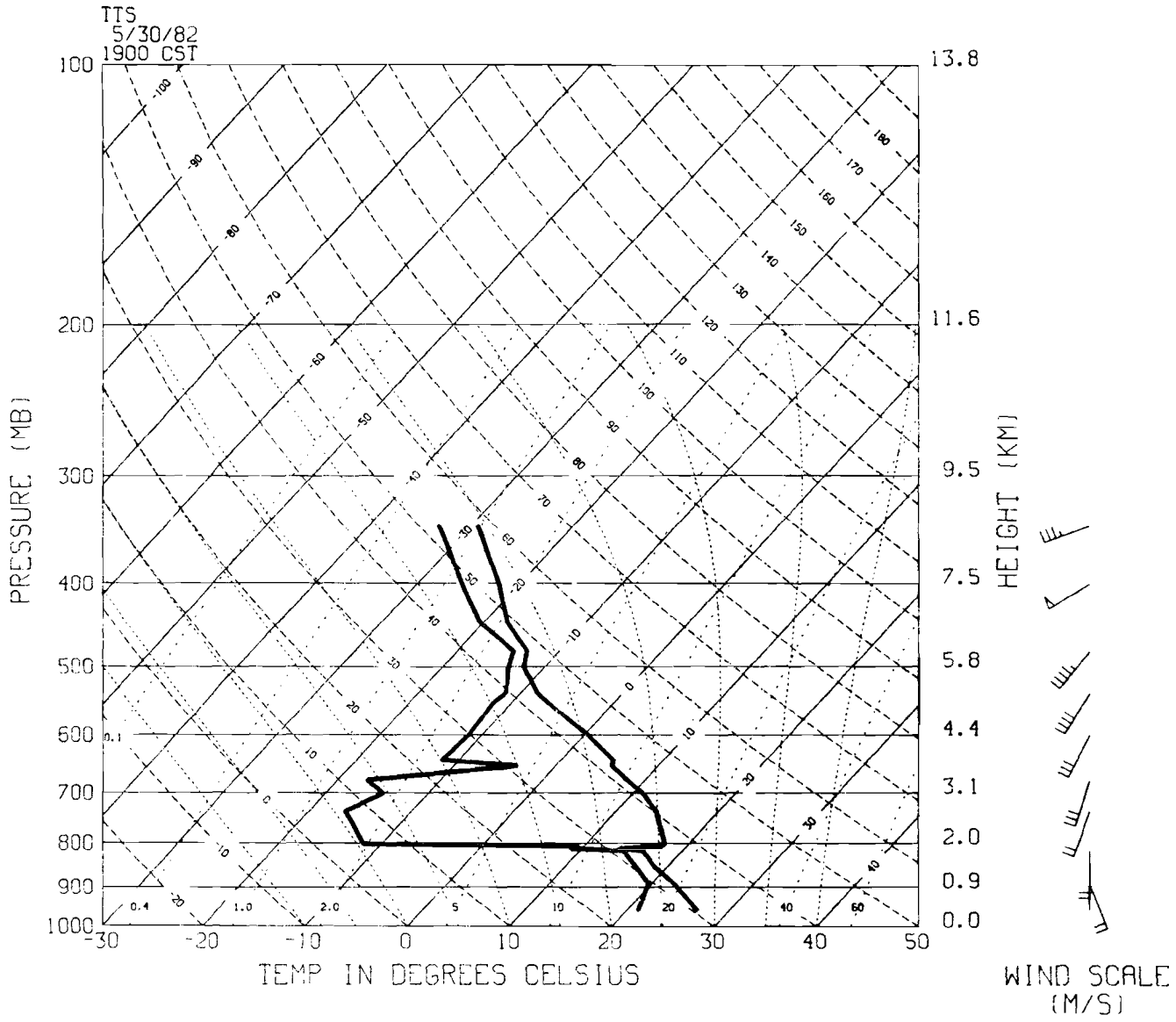

Fig. IV-5(h). Thermodynamic sounding taken at Tuttle (TTS), OK at 1900 CST on 3 May 1982.

F. Case 6: 17 May 1983

1. Synoptic Situation

A dryline extending from eastern Colorado to the Texas Panhandle moved eastward during the day and reached western Oklahoma by evening. Thunderstorms developed along the north end of the dryline in southwest Kansas and built into northwest Oklahoma. A second line developed ahead of the southwest end of the first line and moved over Norman, OK.

2. Doppler Radar Displays

The three spectral moment displays are presented in Figures IV-6(a) through IV-6(c) for 2235 CST. The cursor marks the position of the gust front in the vicinity of the greatest radial shear. (Notice that the sector scan did not include the entire gust front.) There is no indication of the gust front in the reflectivity field (Fig. IV-6(a)), nor is there a clear-cut pattern of enhanced spectrum width (Fig. IV-6(c)), though some enhancement is occurring (label A). The Doppler velocity display shows a noticeable bulge in the outflow near the cursor, which coincides with an area of enhanced reflectivities. In the tilt sequence immediately preceding this volume scan, velocities of 30 ms^{-1} (folded) were present in this region. Some folding is still evident in Fig. IV-6(b) (label B).

3. Thermodynamic Sounding

This gust front continued to move east-northeast at about 19 ms^{-1} and did not cross the WKY-TV tower. Figure IV-6(d) is the sounding taken at Tuttle, OK at 1936 CST, approximately 2 to 3 hours before the storms moved into the area. Low level environmental flow is from the southeast and south. Veering of the winds with height is evident in this case, as in previous cases. A layer of moisture extends from the surface to 800 mb and the lifted index is about -7 with a slight capping inversion at 800 mb.

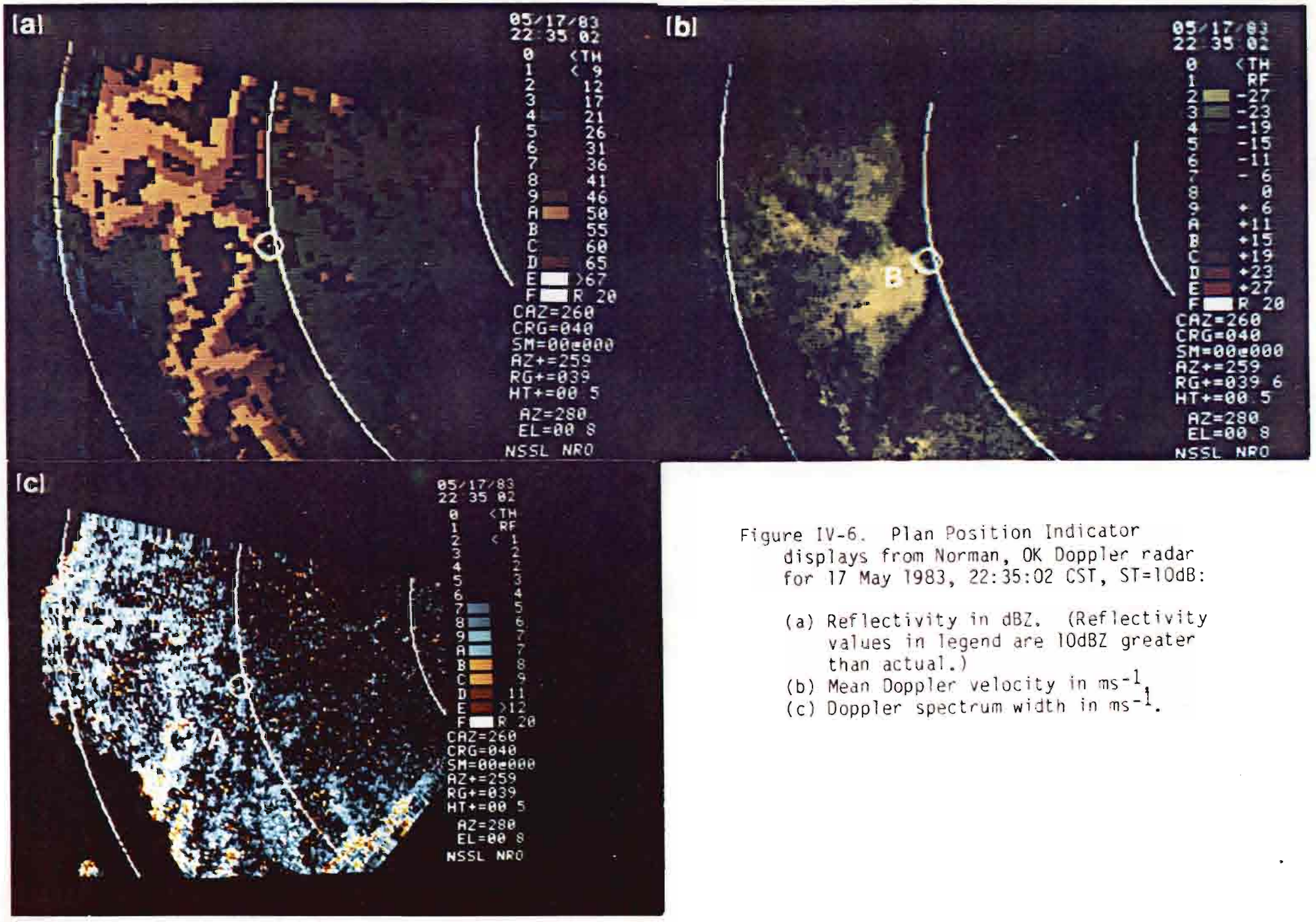

Figure IV-6. Plan Position Indicator displays from Norman, OK Doppler radar for 17 May 1983, 22:35:02 CST, ST=10dB:

(a) Reflectivity in dBZ. (Reflectivity values in legend are 10dBZ greater than actual.)
(b) Mean Doppler velocity in ms^{-1}.
(c) Doppler spectrum width in ms^{-1}.

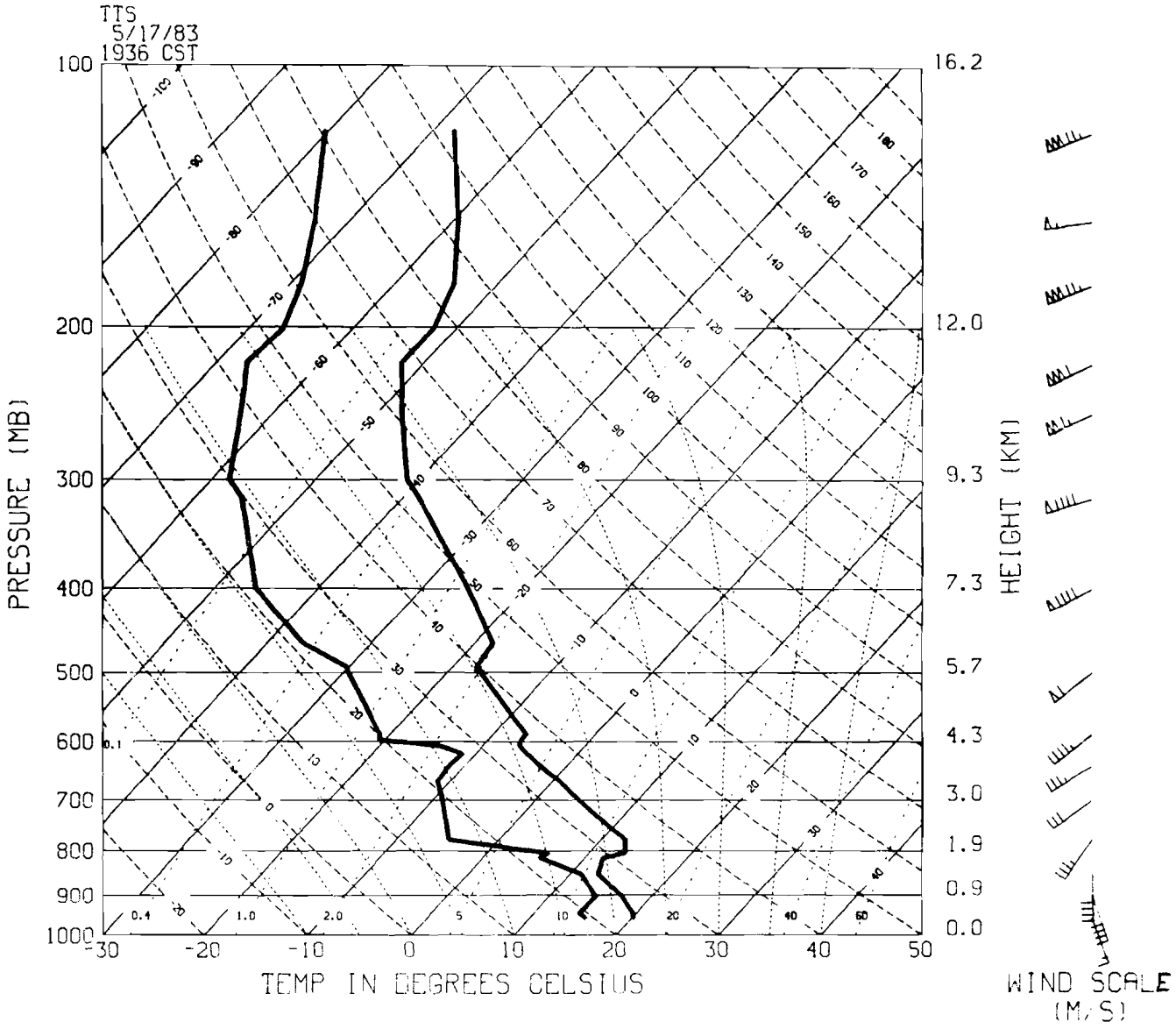

Fig. IV-6(d). Thermodynamic sounding taken at Tuttle (TTS), OK at 1936 CST on 17 May 1983.

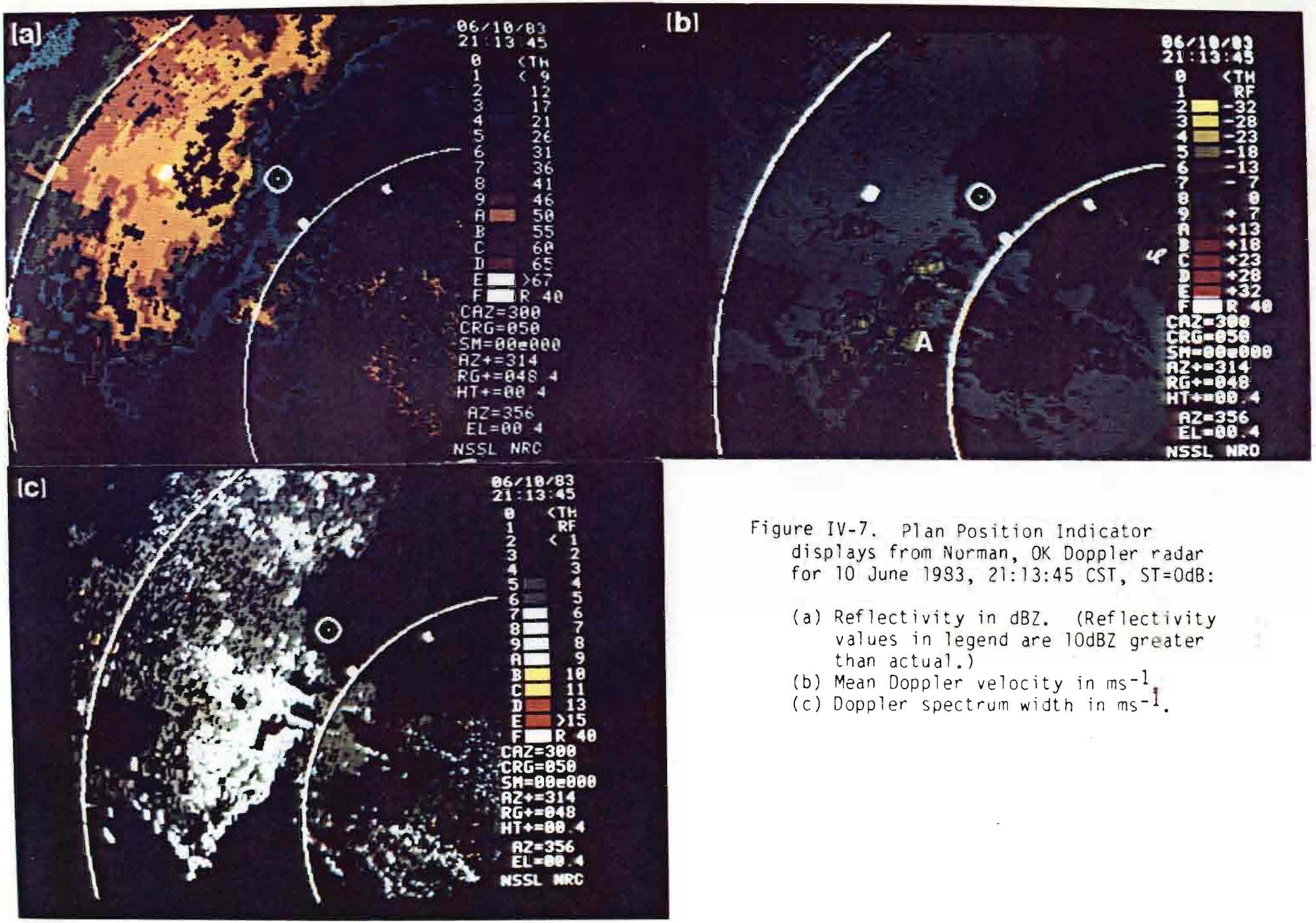

Figure IV-7. Plan Position Indicator displays from Norman, OK Doppler radar for 10 June 1983, 21:13:45 CST, ST=0dB:

(a) Reflectivity in dBZ. (Reflectivity values in legend are 10dBZ greater than actual.)
(b) Mean Doppler velocity in ms^{-1}.
(c) Doppler spectrum width in ms^{-1}.

G. Case 7: 10 June 1983

1. Synoptic Situation

An upper level disturbance and moderately unstable low level conditions combined to form a line of thunderstorms stretching from south central Kansas to the northeast Texas Panhandle. By the time the Doppler radar began scanning this line, the gust front had already formed, separated from the storm, and produced a thin line echo.

2. Doppler Radar Data

This case illustrates how range aliasing can inhibit gust front detection. The cursor marks the position of the thin line echo in the reflectivity field (Fig. IV-7(a)). However, on the velocity (Fig. IV-7(b)) and the spectrum width (Fig. IV-7(c)) displays, the cursor denotes an area of range folding. Returning to the velocity display (Fig. IV-7(b)), one notices that there are only small, isolated areas where the flow has a component along the beam. The velocity field is dominated by zero velocities and the only place one can infer the wind shear across the outflow boundary is in the area labeled A (Fig. IV-7(a)). Even the spectrum width field (Fig. IV-7(c)) does not present a well-defined turbulent region associated with the gust front.

3. Tower Data

The gust front propagated southeast at about 8 ms^{-1} and crossed the tower at 2144 CST (Fig. IV-7(d)). This is evidenced by the change in the streamline pattern, by the cooling in the potential temperature field, and by an increase in all three wind components.

4. Thermodynamic Sounding

Figure IV-7(e) is the sounding taken at Tuttle (TTS), OK at 1901 CST, approximately 2 hours before the line moved into the area. As before, winds veer with height from southeasterly to southwesterly at 500 mb. The lifted index for this sounding is on the order of -5.

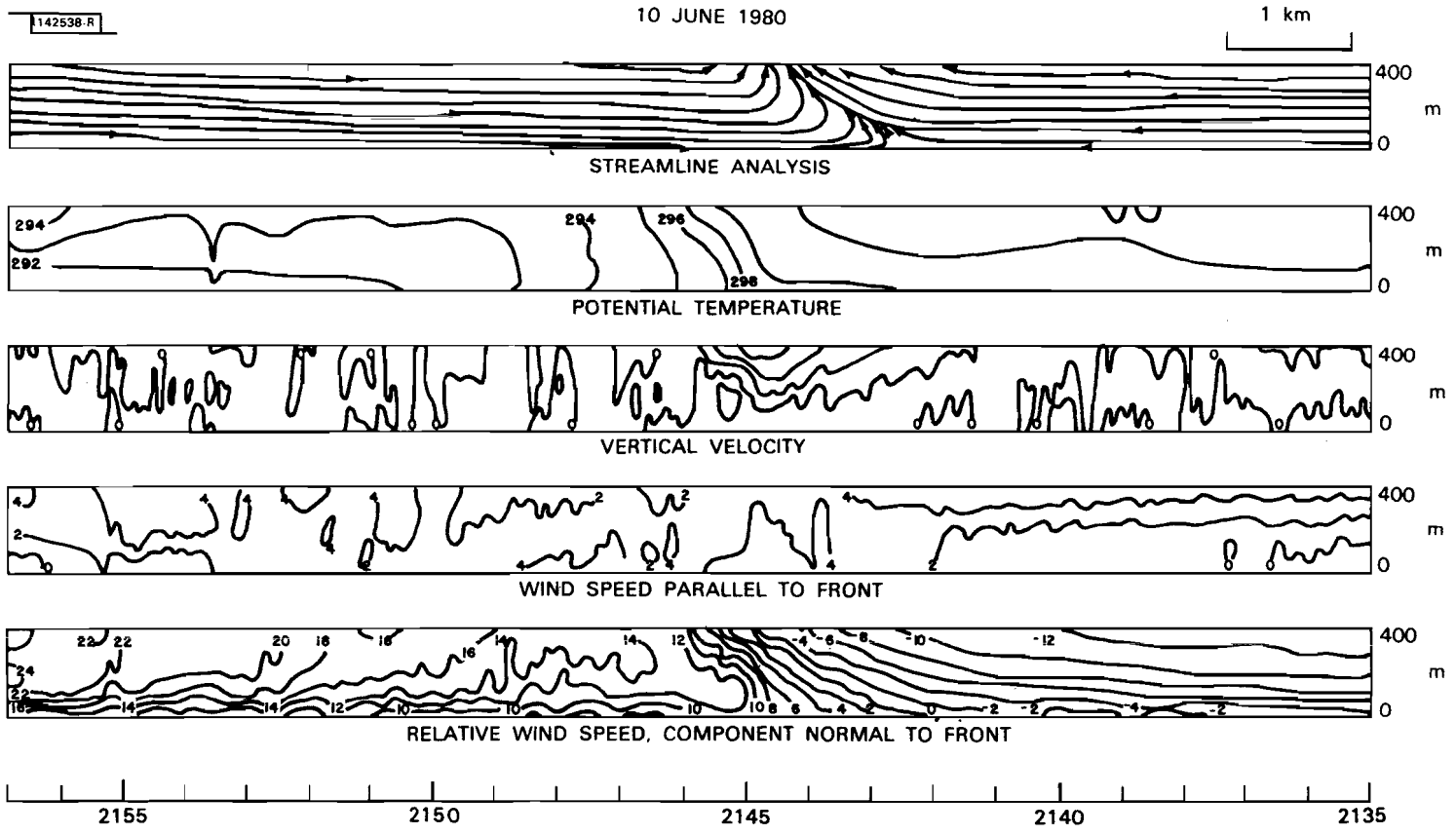

Fig. IV-7(d). Plots of the WKY-TV tower data collected during the passage of the gust front (2135-2156 CST) on 10 June 1983.

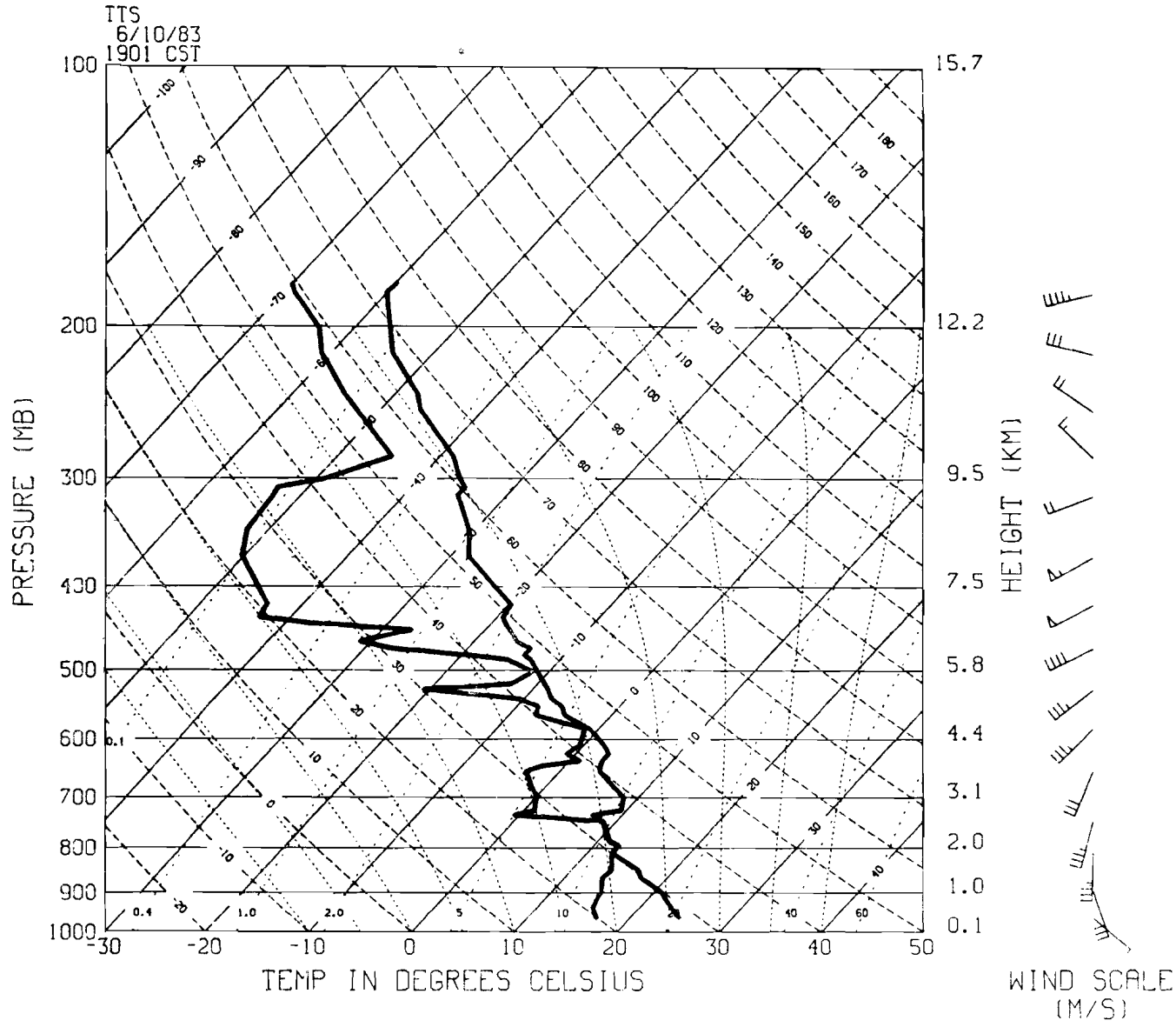

Fig. IV-7(e). Thermodynamic sounding taken at Tuttle (TTS), OK at 1901 CST on 10 June 1983.

H. Case 8: 26 April 1984

The final case presented here involves two gust fronts which were produced at different locations along the same line of storms.

1. Doppler Radar Displays

Figures IV-8(a) through IV-8(c) show the three moment displays of the first gust front produced by this line of storms. This outflow never separated from the storm to produce a thin line echo (Fig. IV-8(a)). The gust front is defined by the strong radial shear pattern in the velocity field (Fig. IV-8(b)) and by the line of enhanced spectrum width (cursor) in Fig. IV-8(c).

Figures IV-8(d) through IV-8(f) show the gust front at the next elevation angle (1.5°). Although the winds behind the outflow leading edge are no longer all inbound (Fig. IV-8(e)), strong radial shear is still found at the boundary. In this case, the spectrum width field (Fig. IV-8(f)) may be more useful in defining the gust front because the pattern is more pronounced. An interesting feature is evident in Fig. IV-8(e) (label A), where the band of inbound velocities is surrounded by outbound velocities. It is believed that the radar beam is cutting through the head of the gust front and sensing environmental winds on either side (roughly from the southwest at 35 ms^{-1}). The location of the radar beam illustrated in Fig. IV-8(q) indicates a possible configuration for that in Fig. IV-8(e). The area of positive velocities (label B) in Fig. IV-8(b) is associated with the higher reflectivities of the precipitation echoes (Fig. IV-8(a), label C) and therefore probably corresponds to the divergent signature of the main storm downdraft.

The line of storms continued to propagate east-northeast and, at about 2040 CST, it became evident that the cell at the south end of the line was producing a second gust front. Figures IV-8(g) through IV-8(i) show the reflectivity, Doppler velocity and spectrum width fields, respectively, for this gust front. The outflow is most well-defined in the reflectivity field (Fig. IV-8(g)) as a thin line echo (cursor) which undercuts the cell at label D. The degree of radial shearing along the outflow boundary (Fig. IV-8(h); cursor) is not large. The only evidence of a gust front in the velocity field is the slight decrease in the negative velocities behind the boundary (e.g., label E).

The large spectrum widths (Fig. IV-8(i)) at labels F and G are due to weak signal. There is no obvious pattern in the spectrum width field that can be directly related to the outflow boundary.

It should be noted that in Figures IV-8(g) through IV-8(i) the threshold of the signal-to-noise ratio (ST) is 0 dB. Figures IV-8(j) through IV-8(l) show the same scan with ST=10 dB. By increasing the

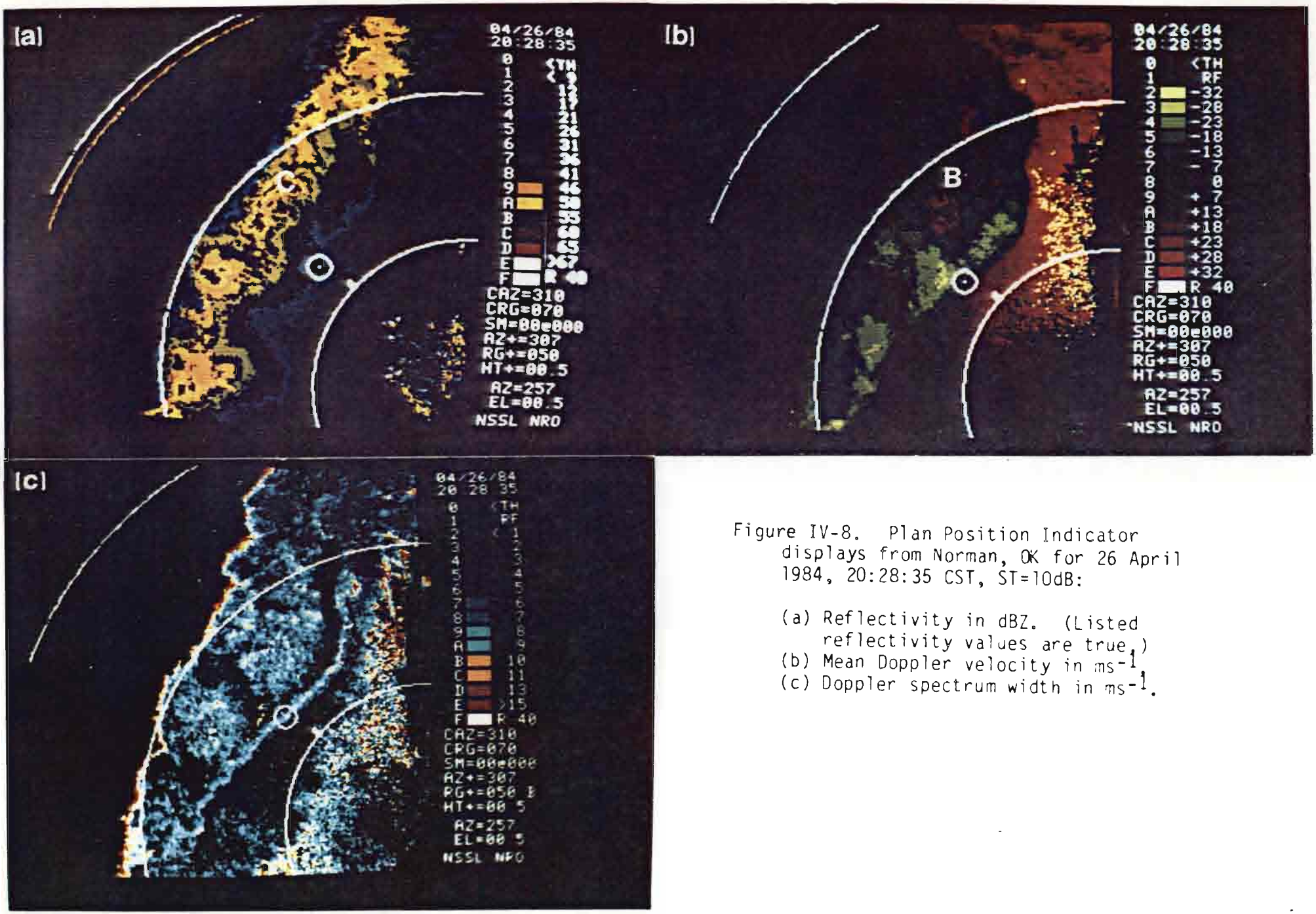

Figure IV-8. Plan Position Indicator displays from Norman, OK for 26 April 1984, 20:28:35 CST, ST=10dB:

(a) Reflectivity in dBZ. (Listed reflectivity values are true.)
(b) Mean Doppler velocity in ms^{-1}.
(c) Doppler spectrum width in ms^{-1}.

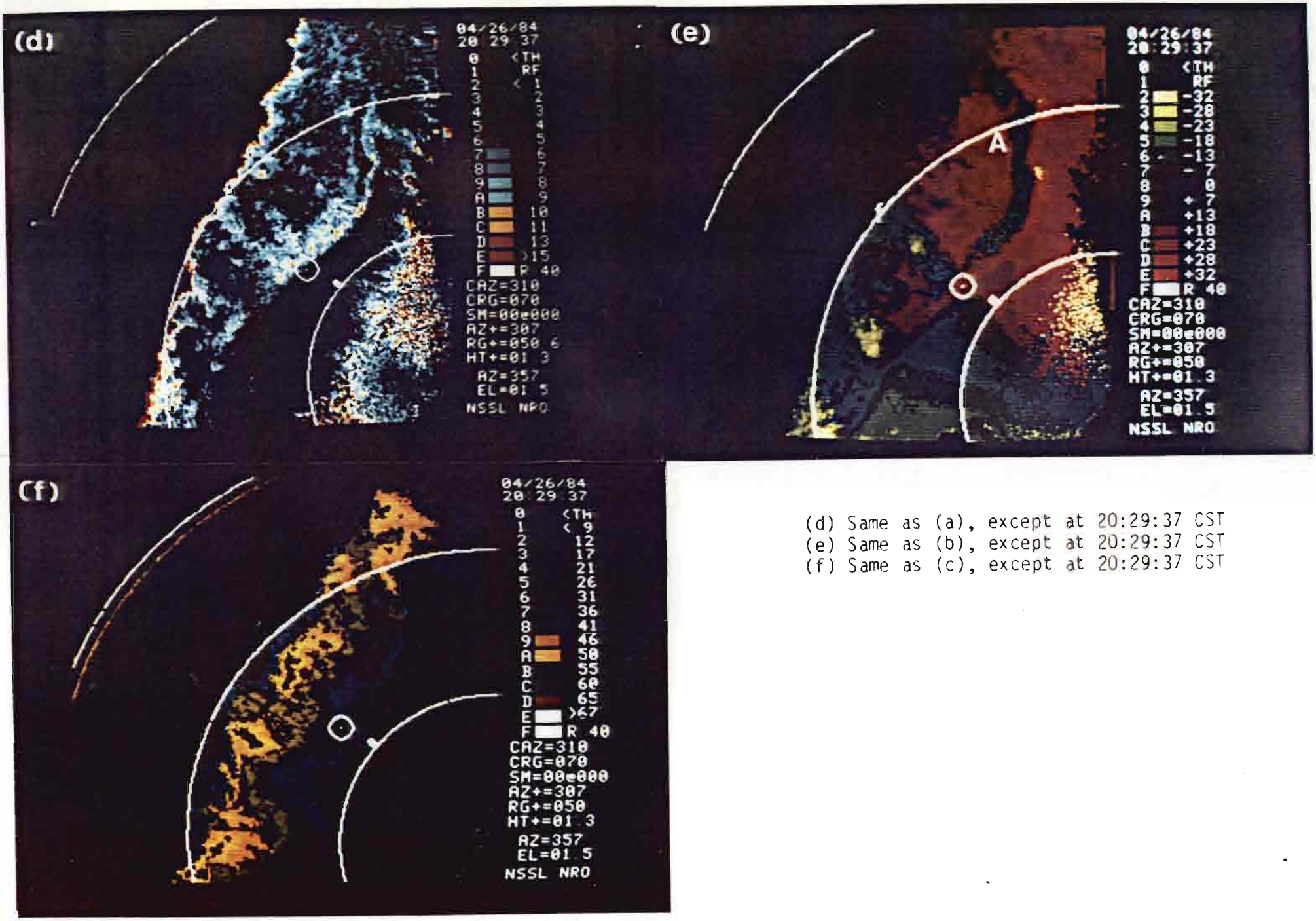

(d) Same as (a), except at 20:29:37 CST
(e) Same as (b), except at 20:29:37 CST
(f) Same as (c), except at 20:29:37 CST

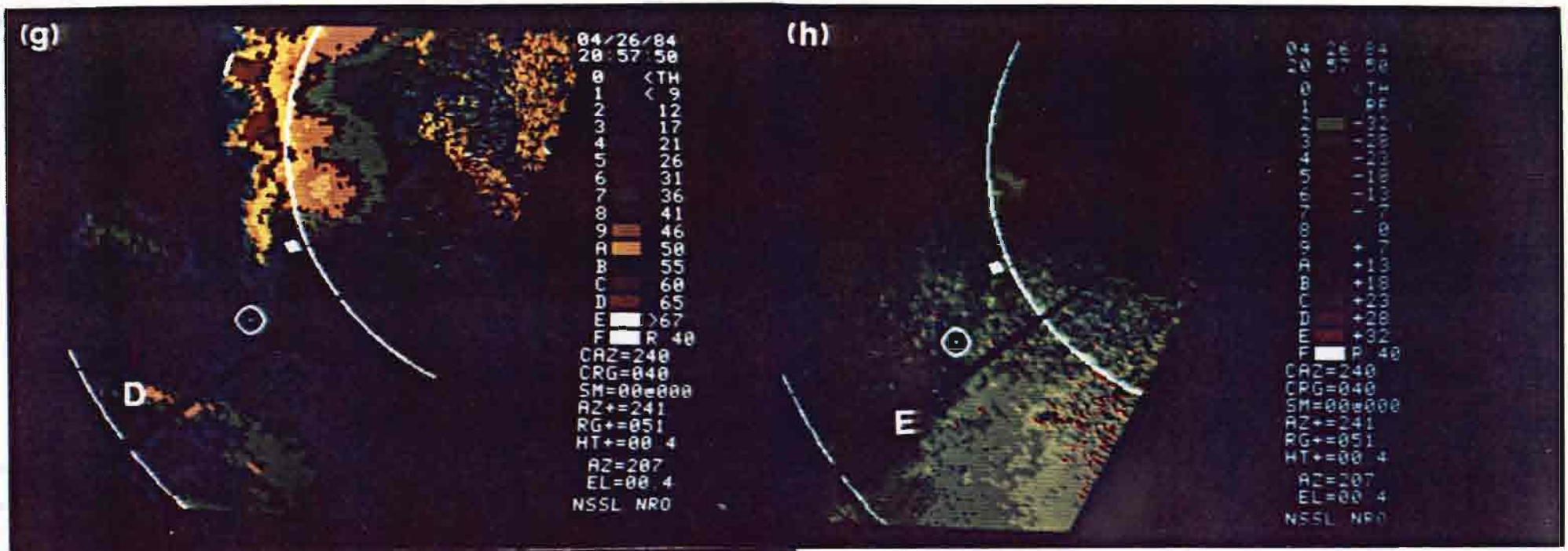

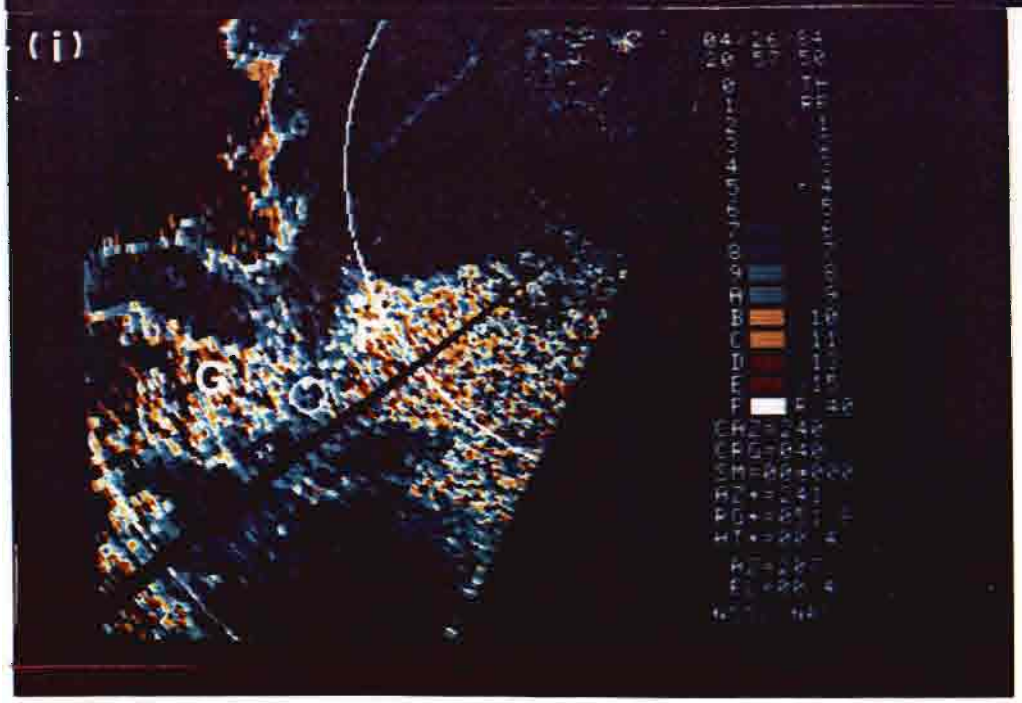

(g) Same as (a), except at 20:57:50 CST (Reflectivity values in legend are 10dBZ greater than actual.)
(h) Same as (b), except at 20:57:50 CST
(i) Same as (c), except at 20:57:50 CST

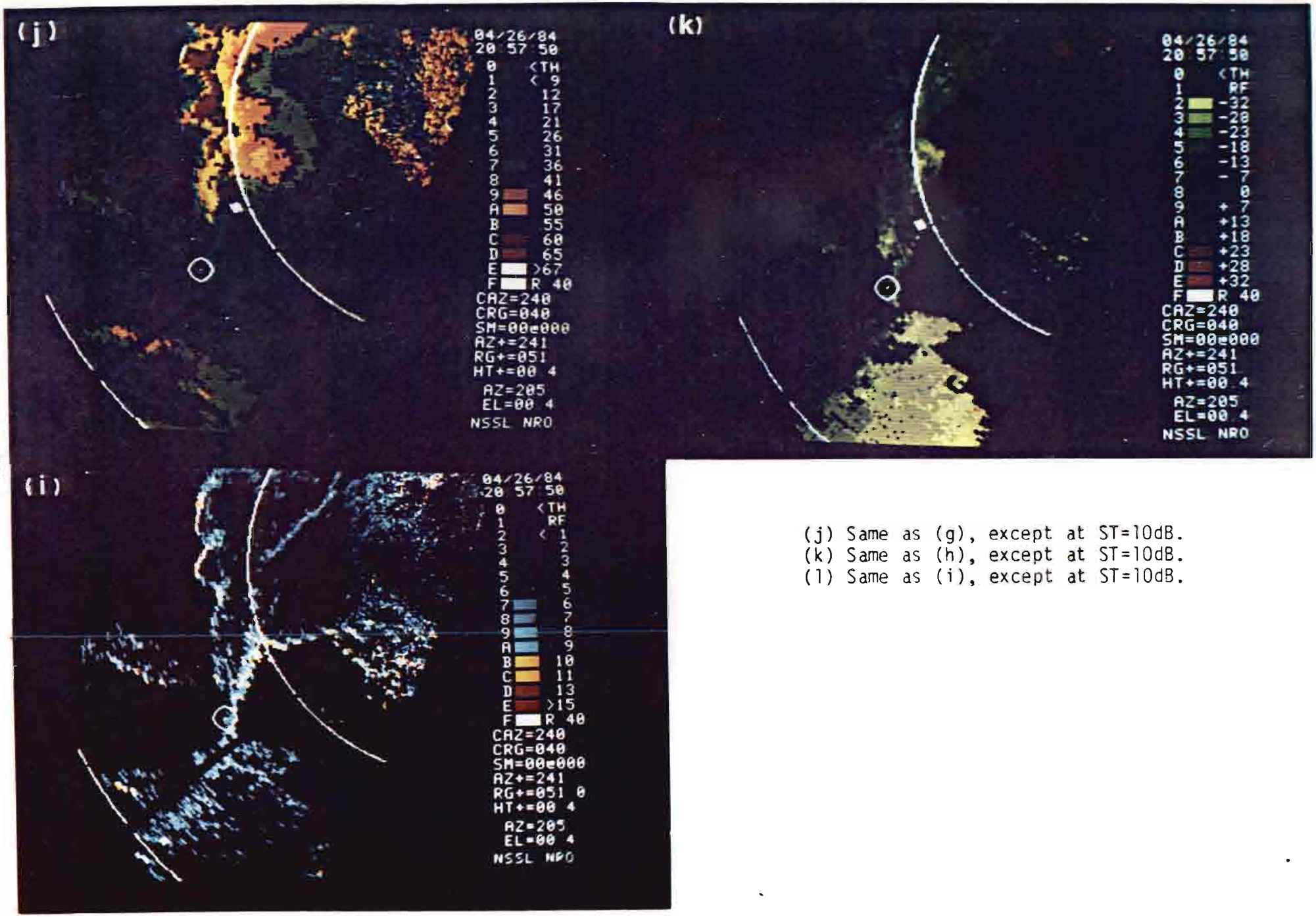

(j) Same as (g), except at ST=10dB.
(k) Same as (h), except at ST=10dB.
(l) Same as (i), except at ST=10dB.

threshold, the clear air signal is removed leaving line features in all three fields. Notice the enhancement of the spectrum width indicative of real turbulence along the gust front (Fig. IV-8(l); cursor).

As the storms propagate to the northeast, the parent cell of the southern gust front continues to create a boundary which moves eastward. Figures IV-8(m) through IV-8(o) show the three spectral moments (ST=0 dB) of the southern gust front about an hour later, after it has moved east of the radar. The thin line echo (Fig. IV-8(m); cursor) is still evident, but a change has taken place in the velocity field (Fig. IV-8(n)). Whereas in previous scans no radial shear could be seen, now a definite shear line has developed (cursor). Winds behind the outflow boundary are outbound (positive) and environmental winds are inbound (negative). A faint linear pattern of enhanced spectrum widths (Fig. IV-8(o); cursor) is discernible. It is interesting to note that this pattern is maintained even where the gust front undercuts a storm cell to the south (label H).

2. Thermodynamic Sounding

Figure IV-8(p) is the sounding taken at Edmond (EDM), OK at 1819 CST which preceded the storm by 2 to 3 hours. As in all previous soundings, the winds veered with height. The lifted index for this case is about -7 with a slight capping inversion.

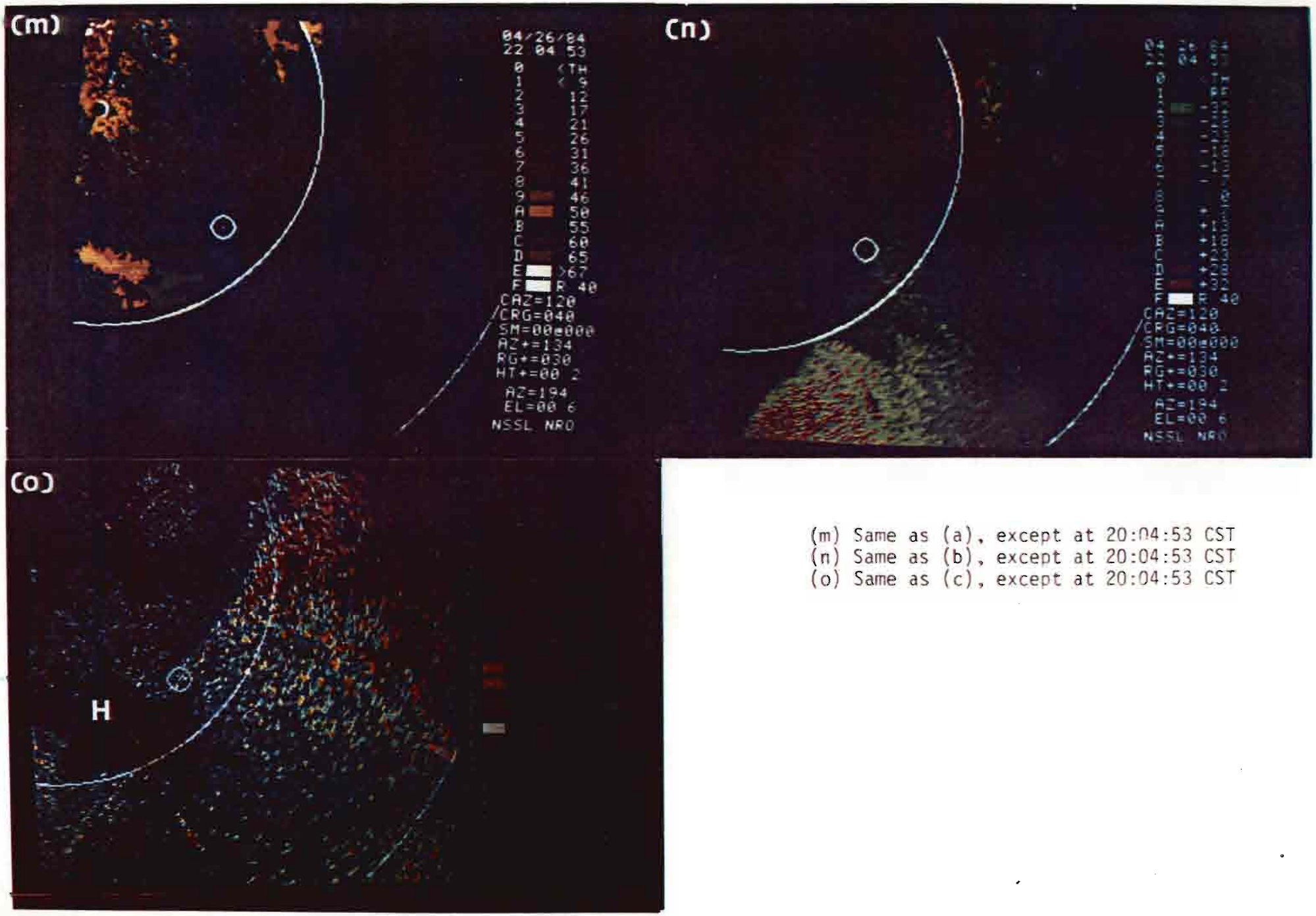

(m) Same as (a), except at 20:04:53 CST
(n) Same as (b), except at 20:04:53 CST
(o) Same as (c), except at 20:04:53 CST

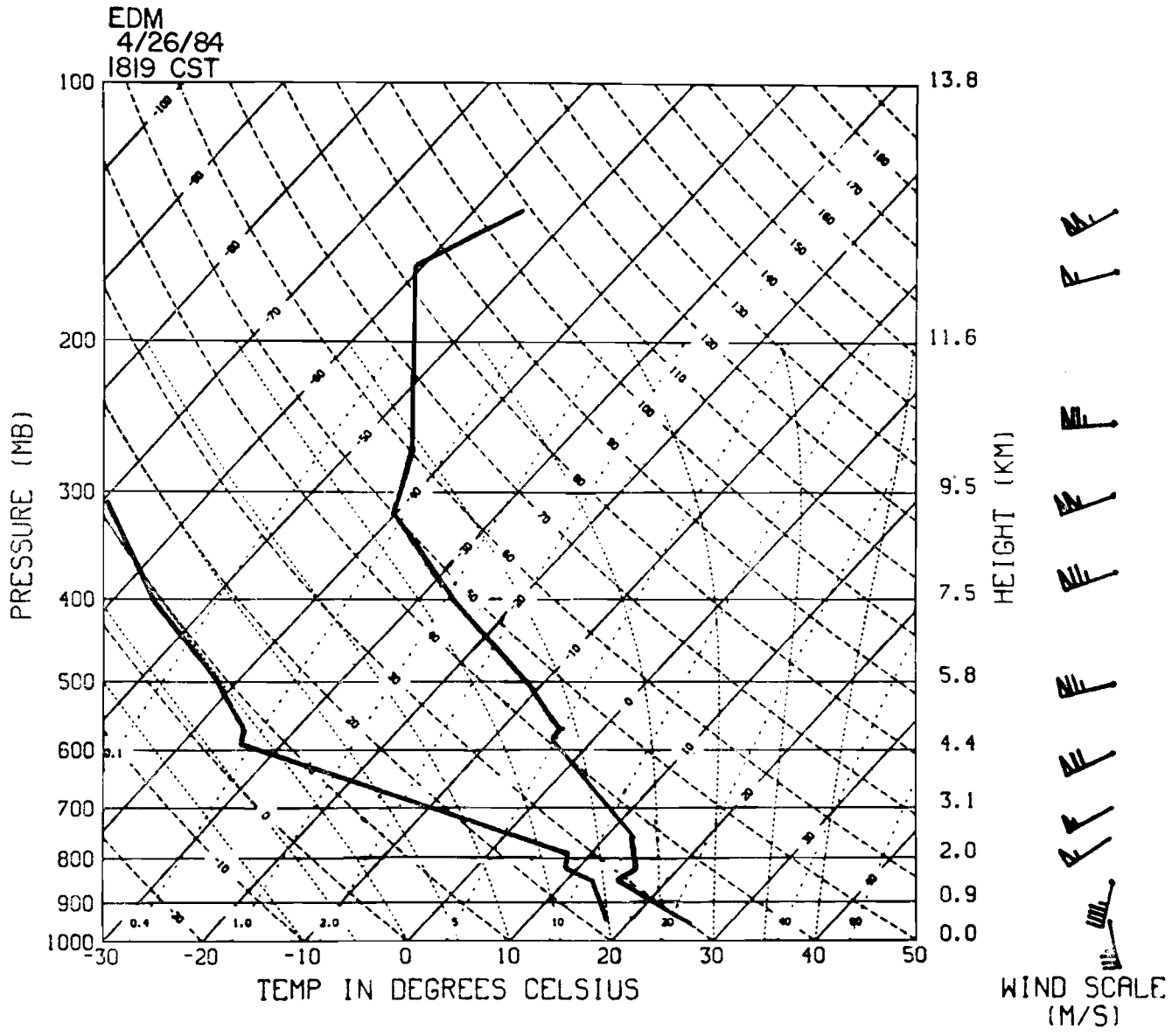

Fig. IV-8(p). Thermodynamic sounding taken at Edmond (EDM), OK at 1819 CST on 26 April 1984.

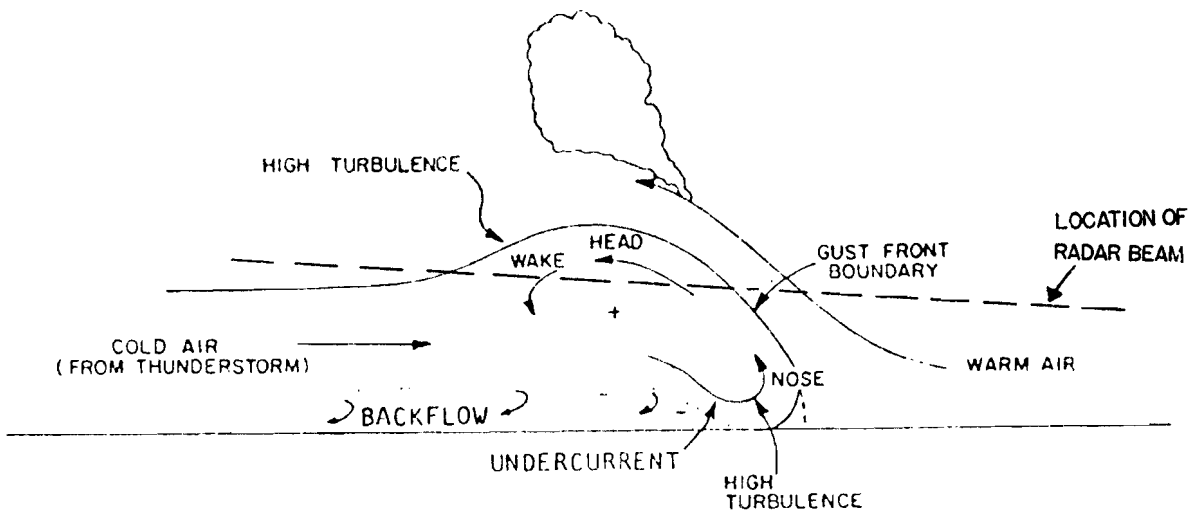

Fig. IV-8(q). Simplified vertical cross-section of a gust front. Streamlines are gust front relative. The path of the radar beam indicates how the inbound velocities within the outflow may be surrounded by outbound velocities in the environmental air as in Fig. IV-8(e). (Adapted from Goff, 1975.)

V. CONCLUSIONS

Eight case studies of gust fronts that occurred in Oklahoma are presented. The Doppler radar at the National Severe Storms Laboratory was used to scan these storm systems. The major findings of this investigation are:

1) Doppler radars are useful in detecting gust fronts which appear as either thin line echoes in the reflectivity fields, linear patterns of radial shear in the Doppler velocity field, lines of enhanced spectrum width or any combination of these three. The frequency of occurrence of these signatures for the ten gust fronts presented in this report are tabulated in Table V-1.

2) Thunderstorm outflows are detected first and most reliably in the Doppler velocity field. The outflow boundary appears as a line of radial convergence (radial shear). In the eight cases presented here, the maximum radial shear is about 12×10^{-3} s^{-1} and the minimum is a threshold value of 0.5×10^{-3} s^{-1}. As the outflow boundary becomes radially oriented with respect to the radar, the shear across the outflow boundary becomes azimuthal instead of radial. No measurements of azimuthal shear were made in this investigation.

3) Gust fronts can be detected in the spectrum width field as linear patterns of enhanced values. Turbulence is present at the interface between the outflow boundary and environmental flow. In some cases, radial orientation of the gust front can prevent its detection in the velocity field, but as Z-L have shown, a line of enhanced spectrum widths may still be evident. If the gust front moves into an area of weak signal, the corresponding increase in the entire spectrum width data field may obliterate any evidence of the gust front pattern. Enhanced spectrum width alone is not reliable for locating gust fronts because the estimated width of velocity spectra can be large due to factors such as range folding and weak signal which are not related to turbulence.

4) In the early stages of development, the gust front is associated with the higher reflectivities of the precipitation echo. Gust fronts have been found in reflectivity fields, but only after they have moved away from the parent storm and formed a thin line echo. Z-L used the 2 dBZ contour to define the gust front echo. For the eight cases presented here, the smallest value of peak reflectivity was 7 dBZ (in agreement with Z-L).

5) The ability to identify gust fronts in clear air on the radar displays is strongly dependent upon the threshold of the signal-to-noise ratio (ST). For instance, comparison of velocity displays at

TABLE V-1

OCCURRENCES OF DOPPLER RADAR SIGNATURES FOR 10 GUST FRONTS

Gust Front	Reflectivity[1]	Velocity[2]	Spectrum Width[3]
30 April 1978 (Northern)	X[4]	X	X[4]
30 April 1978 (Southern)	X[4]	X	X[4]
2 May 1978		X	
19 June 1980	X	X	
15 May 1982	X	X	X
30 May 1982		X	X
17 May 1983	X	X	X
10 June 1983	X		
26 April 1984 (First)		X	X
26 April 1984 (Second)	X	X[4]	X[4]

1. Thin line echo
2. Line of radial shear
3. Line of enhanced spectrum width
4. Not present in first scans, but developed later

5) continued

ST=0 dB and ST=10 dB shows that a significant amount of weak signal is removed at the higher threshold and that the gust front signature in those areas is eliminated. Thus, it is desirable to use a low threshold in order to be able to see the entire outflow boundary. However, as the ST is decreased, the spectrum width field becomes very "noisy" which can lead to obscuration of the gust front signature in this field. So, high thresholds are needed in order for the spectrum width gust front signature to be detected. The root mean square (RMS) error for velocity and spectrum width at SNR=10 dB is 1 ms^{-1} while at SNR=0 dB, the RMS error is 2 ms^{-1} and 3 ms^{-1}, respectively* (Doviak and Zrnic, 1984).

One of the greatest challenges that NEXRAD must face will be to detect and provide adequate warning of low altitude wind shear. Gust fronts that do not separate from the precipitation echo are not dangerous because pilots do not usually fly into high reflectivity areas. As the outflow boundary moves away from the storm, its reflectivity decreases and the gust front becomes more difficult to detect. Relying on reflectivity alone as a measure of the potential hazard is unwise because, as shown here, these low reflectivity outflows can harbor significant, possibly dangerous wind shear. The use of Doppler velocity and spectrum width is essential. Also, the ability to identify hazardous wind shear in its formative stages (i.e., associated with precipitation echo) allows one to track the shear line as its signal strength decreases.

The eight gust front case studies presented in this handbook display many differences as well as similarities. The purpose of this investigation was to define storm outflows in terms of their empirical evidence in the Doppler radar data in order to facilitate the development of automatic gust front detection algorithms. This work, together with Z-L, brackets the range of Oklahoma gust fronts detected by the Norman Doppler radar. It provides, in an easily accessible form, a reference depicting the characteristic features of these phenomena that could reliably be used for their automatic detection and tracking with single Doppler radar. Many of the eight cases presented in this report were also scanned by the Cimmaron Doppler radar. Dual Doppler data are available and analyses of the cases would provide valuable insight into the structure and life cycle of the outflow. The understanding gained from these analyses would improve detection, tracking and prediction capabilities.

*These values were arrived at assuming a spectrum width of 6 ms^{-1}, an unambiguous velocity of 23 ms^{-1} and 32 samples.

REFERENCES

T.B. Benjamin, "Gravity Current and Related Phenomena," J. Fluid Mech., 31 (1968), pp. 209-248.

E.A. Brandes, "Gust Front Evolution in Severe Thunderstorms: Preliminary Investigation with Doppler Radar," Preprints, 7th Conf. on Aerospace and Aeronautical Meteor., Amer. Meteor. Soc., Boston, Massachusetts (1976), pp. 56-61.

H.A. Brown, "Report on Radar Thin Lines," Proc. 8th Wea. Radar Conf., Amer. Meteor. Soc., Boston, Massachusetts (1960), pp. 65-72.

J. Charba, "Gravity Current Model Applied to Analysis of Squall-Line Gust Front," NOAA Tech. Memo. ERL NSSL-61, National Severe Storms Laboratory, Norman, Oklahoma (1972), 58 pp.

J. Charba and Y. Sasaki, "G-Current Model Applied to Analysis of Squall Line Gust Front," Preprints, 7th Conf. on Severe Local Storms, Amer. Meteor. Soc., Boston, Massachusetts (1971), pp. 277-283.

R.J. Doviak and D.S. Zrnic', Doppler Radar and Weather Observations, (Academic Press, Inc., Orlando, Florida, 1984).

M.E. Eilts, personal communication (1984).

T.T. Fujita, "Tornadoes and Downbursts in the Context of Generalized Planetary Scales," J. Atmos. Sci., 38(8) (1981), pp. 1511-1534.

R.C. Goff, "Thunderstorm Outflow Kinematics and Dynamics," NOAA Tech. Memo., ERL NSSL-75 (1975), 63 pp.

R.C. Goff, "Observations of Thunderstorm Induced Low Level Wind Variations," Preprints, Amer. Inst. of Aeronautics and Astronautics, 9th Fluid and Plasma Dynamics Conf., San Diego, California (AIAA Paper No. 76-388, 1976).

J.L. Goldman and P.W. Sloss, "Structure of the Leading Edge of Thunderstorm Cold Air Outflow," Preprints, 6th Conf. on Severe Local Storms, Amer. Meteor. Soc., Boston, Massachusetts (1969), pp. 75-79.

W.G. Harper, "Detection of Bird Migration by Centimetric Radar: A Cause of Radar Angels," Proc. Roy. Soc., B149: 484-502 (1958).

W.G. Harper, "An Unusual Indicator of Convection," Marine Observer, 30: 36-40 (1960).

J.B. Klemp and R.B. Wilhelmson, "Simulations of Right- and Left-Moving Storms Produced Through Storm Splitting," J. Atmos. Sci., 35 (1978), pp. 1097-1110.

J.T. Lee, J. Stokes, Y. Sasaki, and T. Baxter, "Thunderstorm Gust Fronts - Observations and Modeling," FAA Rept. No. FAA-RD-78-145, Dept. of Transportation (1978), 100 pp.

W. Leach, "Observed Characteristics of Convective Cell Bands," Proc. 6th Wea. Radar Conf., Amer. Meteor. Soc., Boston, Massachusetts (1957), pp. 151-156.

G. Luckenback, "Two Examples of Non-Precipitating Echoes as Observed on AN/CPS-9 Radar," Proc. 7th Wea. Radar Conf., Amer. Meteor. Soc., Boston, Massachusetts (1958), pp. D41-D47.

J.E. Simpson, "A Comparison Between Laboratory and Atmospheric Density Currents," Quart., J. Roy. Meteor. Soc., 95 (1969), p. 758-765.

R.M. Wakimoto, "The Life Cycle of Thunderstorm Gust Fronts as Viewed by Doppler Radar and Rawinsonde Data," Mon. Wea. Rev. 110(8) (1982), pp. 1060-1082.

D.S. Zrnic' and J.T. Lee, "Investigation of the Detectability and Lifetime of Gust Fronts and other Weather Hazards to Aviation," FAA Final Rept. No. DOT/FAA/PM-83/33 (1983), 58 pp.

D.S. Zrnic' and H. Uyeda, personal communication (1984).

APPENDIX A

Gust Front Characteristics

This appendix contains tables of gust front characteristics computed by interactively using the NSSL color displays and cursor. Listed below are explanations of the categories tabulated on the following pages.

Time - beginning time of tilt in hours, minutes and seconds (HHMMSS) CST.

Elevation - elevation angle of the radar antenna in degrees.

Height - height (km) of the cursor at the point along the discernible gust front which is most distant from the radar.

Length - length (km) of outflow leading edge that is discernible on the Doppler radar displays.

Radial Wind Speed in Outflow - magnitude (ms^{-1}) and radial direction (+ or -) of the maximum, minimum and average radial winds within the outflow in the immediate vicinity of the leading edge.

Distance from Max Wind to Outflow Boundary - perpendicular distance between the area of maximum wind speed in the outflow to the boundary separating outflow and environmental air.

Reflectivity Along Gust Front - maximum and minimum reflectivity (dBZ) along the leading edge of the outflow.

Spectrum Width Associated with Gust Front - maximum, minimum and average values of spectrum width (ms^{-1}) along the leading edge.

Signal-to-Noise Threshold - value of the signal-to-noise ratio (dB) below which no data is displayed.

Distance from Gust Front to Generating Storm - shortest distance (km) between the center of the generating storm and the gust front. In cases of lines of reflectivity in which no parent cell was distinguishable, this distance represents the average perpendicular distance between the center of the line and the gust front.

Reflectivity Gradient of Generating Storm - gradient ($dBZ \cdot km^{-1}$) of the reflectivity field at the leading edge of the storm.

Distance from Gust Front to Radar - distance (km) between the Norman Doppler radar and the closest point of the gust front.

TABLE A-1

GUST FRONT CHARACTERISTICS

30 APRIL 1978
(Northern Gust Front)

Time (HHMMSS)	Elevation Angle (deg)	Height (km)	Length (km)	Radial Wind Speed in Outflow (ms^{-1})			Distance from Max Wind to Outflow Boundary (km)	Reflectivity Along Gust Front (dBZ)		Spectrum Width Associated with Gust Front (ms^{-1})			Signal-to-Noise (dB) Threshold	Distance from Gust Front to Generating Storm (km)	Reflectivity ($dBZ \cdot km^{-1}$) Gradient of Generating Storm	Distance from Gust Front to Radar (km)
				Max	Min	Avg		Max	Min	Max	Min	Avg				
202832	0.3	0.2	6.6	-18	-7	-13	3	11	2	6	2	5	10	13	10	45
202933	0.7	0.6	11.1	-18	-7	-13	4	16	2	8	<1	6	10	11	14	44
203034	1.5	1.3	14.7	-18	0	-13	2	40	2	8	<1	4	10	1	21	44
203134	3.0	2.5	9.0	-18	-7	-13	1	55	7	13	<1	4	10	1	13	46
204058	0.3	0.2	23.7	-13	0	-7	1	36	2	8	3	6	0	9	13	36
204200	0.7	0.6	23.9	-32	0	-7	1	55	7	8	2	5	0	2	7	36
204301	1.5	1.2	33.7	-18	0	-13	1	50	-1	13	<1	3	0	3	12	37
204402	3.0	2.5	20.4	-23	-8	-13	1	50	2	8	<1	5	0	2	8	40
205325	0.3	0.1	24.2	-28	0	-7	5	31	-1	8	<1	5	0	17	8	31
205426	0.7	0.4	17.1	-18	0	-7	1	40	7	8	<1	6	0	5	10	31
205527	1.5	1.0	19.8	-18	0	-7	0	40	2	13	<1	5	0	5	11	33

TABLE A-1

GUST FRONT CHARACTERISTICS

30 APRIL 1978 (cont.)

Time (HHMMSS)	Elevation Angle (deg)	Height (km)	Length (km)	Radial Wind Speed in Outflow (ms^{-1})			Distance from Max Wind to Outflow Boundary (km)	Reflectivity Along Gust Front (dBZ)		Spectrum Width Associated with Gust Front (ms^{-1})			Signal-to-Noise (dB) Threshold	Distance from Gust Front to Generating Storm (km)	Reflectivity ($dBZ \cdot km^{-1}$) Gradient of Generating Storm	Distance from Gust Front to Radar (km)
				Max	Min	Avg		Max	Min	Max	Min	Avg				
205628	3.0	1.9	17.5	-18	0	-7	2	36	-1	8	2	6	0	3	6	37
205730	5.0	3.7	16.1	-18	0	-7	0	45	2	not available			0	2	10	34
210551	0.3	0.1	19.1	-23	0	-7	1	16	2	"	"	"	0	3	19	29
210652	0.7	0.3	21.4	-18	0	-7	0	26	11	"	"	"	0	6	18	25
210753	1.5	0.9	17.9	-23	0	-7	0	21	2	"	"	"	0	9	15	25
210855	3.0	1.8	20.2	-23	0	-7	0	21	-1	"	"	"	0	3	15	27
210956	5.0	3.2	15.5	-28	-7	-13	2	45	-1	"	"	"	0	2	15	27

TABLE A-2

GUST FRONT CHARACTERISTICS

30 APRIL 1978
(Southern Gust Front)

Time (HHMMSS)	Elevation Angle (deg)	Height (km)	Length (km)	Radial Wind Speed in Outflow (ms^{-1})			Distance from Max Wind to Outflow Boundary (km)	Reflectivity Along Gust Front (dBZ)		Spectrum Width Associated with Gust Front (ms^{-1})			Signal-to-Noise (dB) Threshold	Distance from Gust Front to Generating Storm (km)	Reflectivity ($dBZ \cdot km^{-1}$) Gradient of Generating Storm	Distance from Gust Front to Radar (km)
				Max	Min	Avg		Max	Min	Max	Min	Avg				
202832	0.3	0.5	28.9	-18	0	-7	3	26	7	10	<1	4	10	9	5	55
202933	0.7	1.1	30.0	-18	0	-7	3	40	21	8	<1	4	10	9	5	55
203034	1.5	2.1	26.8	-28	0	-7	4	45	31	8	<1	4	10	6	3	55
204058	0.3	0.4	50.4	-28	0	-13	2	40	7	13	<1	7	0	9	6	44
204200	0.7	0.9	54.6	-28	0	-13	2	40	7	10	<1	6	0	10	6	45
204301	1.5	1.8	33.0	-28	-7	-18	3	31	-1	13	<1	5	0	9	5	45
205325	0.3	0.4	54.0	-32	0	-18	6	36	-1	11	5	9	0	6	5	30
205426	0.7	0.8	46.5	-32	0	-18	2	31	7	10	<1	7	0	7	7	29
205527	1.5	1.5	46.8	-32	0	-18	5	16	-1	13	<1	8	0	9	10	31
205628	3.0	1.6	24.8	-23	-7	-13	6	36	-1	13	3	6	0	8	6	31
205730	5.0	3.5	24.4	-28	-7	-7	6	45	11	not available			0	7	11	32

TABLE A-2

GUST FRONT CHARACTERISTICS

30 APRIL 1978 (cont.)

Time (HHMMSS)	Elevation Angle (deg)	Height (km)	Length (km)	Radial Wind Speed in Outflow (ms^{-1})			Distance from Max Wind to Outflow Boundary (km)	Reflectivity Along Gust Front (dBZ)		Spectrum Width Associated with Gust Front (ms^{-1})			Signal-to-Noise (dB) Threshold	Distance from Gust Front to Generating Storm (km)	Reflectivity ($dBZ \cdot km^{-1}$) Gradient of Generating Storm	Distance from Gust Front to Radar (km)
				Max	Min	Avg		Max	Min	Max	Min	Avg				
210551	0.2	0.4	69.4	-28	0	-18	4	21	2	"	"	"	0	11	8	22
210652	0.7	0.6	55.4	-28	0	-18	3	36	7	"	"	"	0	11	8	19
210753	1.5	0.9	30.2	-32	-7	-18	5	21	2	"	"	"	0	11	12	18
210855	3.0	1.8	33.4	-36	0	-18	1	31	2	not available			0	5	8	17
210956	5.0	2.5	35.2	-36	-7	-23	4	36	-1	"	"	"	0	9	8	16
211057	7.0	3.9	40.6	-36	-7	-28	4	31	2	"	"	"	0	3	5	15
Gust Front Passed Radar																
212121	3.0	1.9	64.0	-23	0	-7	0	45	2	"	"	"	0	7	5	0
212222	5.0	3.1	60.1	-23	0	0	0	36	2	"	"	"	0	5	5	0

TABLE A-2

GUST FRONT CHARACTERISTICS

30 APRIL 1978 (cont.)

Time (HHMMSS)	Elevation Angle (deg)	Height (km)	Length (km)	Radial Wind Speed in Outflow (ms^{-1})			Distance from Max Wind to Outflow Boundary (km)	Reflectivity Along Gust Front (dBZ)		Spectrum Width Associated with Gust Front (ms^{-1})			Signal-to-Noise (dB) Threshold	Distance from Gust Front to Generating Storm (km)	Reflectivity ($dBZ \cdot km^{-1}$) Gradient of Generating Storm	Distance from Gust Front to Radar (km)
				Max	Min	Avg		Max	Min	Max	Min	Avg				
212324	7.0	4.2	54.0	-28	-7	-7	0	40	-1	"	"	"	0	3	5	0
221643*	0.3	0.7	105.6	+28	+7	+7	0	16	-1	"	"	"	0	39	1	48
221844	1.4	2.0	87.1	+13	0	0	0	16	-1	"	"	"	0	39	11	50

*Approximately one hour after previous scan.

TABLE A-3

GUST FRONT CHARACTERISTICS

2 MAY 1978

Time (HHMMSS)	Elevation Angle (deg)	Height (km)	Length (km)	Radial Wind Speed in Outflow (ms^{-1})			Distance from Max Wind to Outflow Boundary (km)	Reflectivity Along Gust Front (dBZ)		Spectrum Width Associated with Gust Front (ms^{-1})			Signal-to-Noise (dB) Threshold	Distance from Gust Front to Generating Storm (km)	Reflectivity ($dBZ \cdot km^{-1}$) Gradient of Generating Storm	Distance from Gust Front to Radar (km)
				Max	Min	Avg		Max	Min	Max	Min	Avg				
170513	0.3	0.9	94.6	-13	0	-5	4	36	11	7	3	5	10	13	4	56
170633	0.7	1.1	87.0	-5	0	0	2	40	16	7	3	5	10	10	1	54
173844	0.3	0.3	64.3	-16	0	-9	4	50	21	7	<1	5	10	15	2	23
174003	0.7	0.6	51.5	-16	-5	-9	4	50	26	6	<1	4	10	10	2	23
174122	1.4	0.9	41.0	-9	0	-5	3	50	26	7	<1	4	10	9	2	21
175850	0.3	0.1	39.0	+5	0	+5	0	50	2	6	<1	2	10	11	2	0
180010	0.7	0.7	33.7	+9	0	+5	0	36	26	6	<1	2	10	8	2	3
180128	1.4	0.7	57.5	+5	0	+5	0	45	21	6	<1	2	10	7	1	3
180247	2.3	0.8	33.1	+13	0	+5	2	45	21	6	<1	2	10	8	1	4
180532	0.3	0.1	39.1	+9	0	+5	0	50	21	5	<1	4	10	11	3	5
180651	0.7	0.7	56.5	+13	0	+9	3	50	11	5	<1	4	10	8	3	11

TABLE A-3

GUST FRONT CHARACTERISTICS

2 MAY 1978 (cont.)

Time (HHMMSS)	Elevation Angle (deg)	Height (km)	Length (km)	Radial Wind Speed in Outflow (ms^{-1})			Distance from Max Wind to Outflow Boundary (km)	Reflectivity Along Gust Front (dBZ)		Spectrum Width Associated with Gust Front (ms^{-1})			Signal-to-Noise (dB) Threshold	Distance from Gust Front to Generating Storm (km)	Reflectivity ($dBZ \cdot km^{-1}$) Gradient of Generating Storm	Distance from Gust Front to Radar (km)
				Max	Min	Avg		Max	Min	Max	Min	Avg				
180810	1.4	0.4	27.3	+13	0	+9	3	40	26	5	<1	4	10	7	3	1
181214	0.3	0.2	105.3	+13	0	+9	0	26	16	9	<1	5	10	N/A	3	7
181333	0.7	0.6	70.3	+13	0	+9	6	30	11	7	<1	4	10	N/A	2	11
181453	1.4	0.5	41.4	+9	0	+5	4	31	21	7	<1	4	10	N/A	2	14
183902	0.3	1.1	197.2	+7	0	+4	0	50	-1	9	2	5	10	N/A	2	35

TABLE A-4

GUST FRONT CHARACTERISTICS

19 JUNE 1980

Time (HHMMSS)	Elevation Angle (deg)	Height (km)	Length (km)	Radial Wind Speed in Outflow (ms^{-1})			Distance from Max Wind to Outflow Boundary (km)	Reflectivity Along Gust Front (dBZ)		Spectrum Width Associated with Gust Front (ms^{-1})			Signal-to-Noise (dB) Threshold	Distance from Gust Front to Generating Storm (km)	Reflectivity (dBZ·km^{-1}) Gradient of Generating Storm	Distance from Gust Front to Radar (km)
				Max	Min	Avg		Max	Min	Max	Min	Avg				
220711	0.4	0.4	31.4	-28	0	-7	0	31	-1	13	<1	9	0	11	8	41
221803	0.6	0.3	52.3	-28	0	-13	1	45	-1	>15	<1	6	0	0	1	33
222157	0.4	0.2	26.0	-18	0	-13	5	>57	7	10	2	6	0	2	N/A	31
222208	0.8	0.4	21.2	-18	0	-13	3	>57	7	10	2	6	0	11	"	32
222221	1.2	0.6	22.9	-13	0	-7	2	40	2	9	4	5	0	7	"	32
222234	1.7	1.0	16.3	-13	0	-7	1	40	26	6	<1	4	0	8	"	35
222250	2.4	1.5	6.0	-7	0	-7	0	40	31	4	<1	2	0	8	"	36
222846	0.0	0.0	19.8	-23	0	-13	5	55	7	13	<1	4	0	12	"	26
222854	0.4	0.2	17.5	-23	-7	-13	4	50	7	10	2	4	0	16	4	27
222907	0.9	0.4	17.9	-18	0	-13	5	26	7	10	3	4	0	19	5	27
222920	1.3	0.6	18.2	-18	0	-7	2	31	11	10	4	5	0	19	3	27

TABLE A-4

GUST FRONT CHARACTERISTICS

19 JUNE 1980 (cont.)

Time (HHMMSS)	Elevation Angle (deg)	Height (km)	Length (km)	Radial Wind Speed in Outflow (ms^{-1})			Distance from Max Wind to Outflow Boundary (km)	Reflectivity Along Gust Front (dBZ)		Spectrum Width Associated with Gust Front (ms^{-1})			Signal-to-Noise (dB) Threshold	Distance from Gust Front to Generating Storm (km)	Reflectivity ($dBZ \cdot km^{-1}$) Gradient of Generating Storm	Distance from Gust Front to Radar (km)
				Max	Min	Avg		Max	Min	Max	Min	Avg				
222934	2.1	1.1	18.6	-13	0	0	1	36	11	11	2	4	0	21	10	28
223432	0.4	0.2	21.5	-18	0	-13	7	26	7	10	2	5	0	20	5	23
223444	0.9	0.3	21.5	-23	0	-13	3	31	7	13	2	5	0	18	8	23
223456	1.3	0.6	13.9	-18	0	-13	5	26	7	13	<1	4	0	18	6	23
223506	2.0	1.1	18.7	-13	0	-7	1	36	11	8	2	3	0	13	7	25
224047	0.5	0.2	17.2	-13	0	-7	3	36	7	8	3	6	0	11	7	20
224059	0.9	0.3	18.1	-18	0	-7	2	16	7	8	4	6	0	13	5	19
224110	1.2	0.4	13.8	-13	0	-7	2	21	7	7	4	6	0	12	11	19
224122	2.1	0.7	17.0	-13	0	-7	3	31	7	7	4	6	0	6	11	19

TABLE A-5

GUST FRONT CHARACTERISTICS

15 MAY 1982

Time (HHMMSS)	Elevation Angle (deg)	Height (km)	Length (km)	Radial Wind Speed in Outflow (ms^{-1})			Distance from Max Wind to Outflow Boundary (km)	Reflectivity Along Gust Front (dBZ)		Spectrum Width Associated with Gust Front (ms^{-1})			Signal-to-Noise (dB) Threshold	Distance from Gust Front to Generating Storm (km)	Reflectivity ($dBZ \cdot km^{-1}$) Gradient of Generating Storm	Distance from Gust Front to Radar (km)
				Max	Min	Avg		Max	Min	Max	Min	Avg				
192735	0.8	1.9	26.6	-18	0	-7	3	50	-1	10	3	7	0	11	4	79
192817	1.2	2.5	29.3	-18	0	-7	2	50	2	10	4	8	0	11	4	79
193101	0.4	1.1	45.5	-18	0	-7	4	50	-1	10	4	8	0	8	5	74
193140	0.8	2.1	42.8	-18	0	-7	1	50	-1	11	4	7	0	7	5	75
193221	1.2	2.7	44.1	-23	0	-7	0	50	-1	11	4	7	0	9	4	80
193505	0.4	1.3	38.7	-18	0	-7	0	45	-1	13	3	6	0	0	4	72
193545	0.8	1.9	38.4	-18	0	-7	0	45	-1	13	4	6	0	4	5	72
193626	1.2	2.1	34.2	-18	0	-7	6	45	-1	11	<1	6	0	5	5	73
193911	0.4	1.1	41.5	-18	0	-7	3	40	-1	13	2	7	0	14	5	65
193949	0.8	1.7	35.8	-18	0	-7	0	40	-1	10	2	6	0	12	4	67
194030	1.2	2.3	19.9	-18	0	-7	1	36	0	13	2	7	0	12	6	67

TABLE A-5

GUST FRONT CHARACTERISTICS

15 MAY 1982 (cont.)

Time (HHMMSS)	Elevation Angle (deg)	Height (km)	Length (km)	Radial Wind Speed in Outflow (ms^{-1})			Distance from Max Wind to Outflow Boundary (km)	Reflectivity Along Gust Front (dBZ)		Spectrum Width Associated with Gust Front (ms^{-1})			Signal-to-Noise (dB) Threshold	Distance from Gust Front to Generating Storm (km)	Reflectivity ($dBZ \cdot km^{-1}$) Gradient of Generating Storm	Distance from Gust Front to Radar (km)
				Max	Min	Avg		Max	Min	Max	Min	Avg				
194315	0.4	1.2	46.2	-28	0	-7	0	36	-1	11	3	7	0	12	5	61
194345	0.8	1.7	34.4	-18	0	-7	1	36	-1	13	4	7	0	15	4	63
194434	1.2	2.2	30.8	-13	0	-7	4	36	-1	9	4	6	0	17	4	65
194720	0.4	1.2	48.5	-18	-7	-7	5	45	-1	13	4	8	0	1	6	59
194804	0.8	1.7	46.5	-18	-7	-7	2	45	-1	13	4	8	0	3	4	59
194840	0.2	2.6	46.1	-13	0	-7	2	45	-1	10	2	7	0	2	4	59
195125	0.4	1.2	52.0	-32	0	-7	1	45	-1	13	3	8	0	0	6	56
195201	0.8	1.7	33.4	-18	0	-7	0	45	-1	13	<1	9	0	3	4	65
195245	1.2	2.0	40.0	-13	0	-7	1	50	-1	13	<1	6	0	1	6	59
195530	0.4	1.2	48.0	-18	0	-7	1	50	-1	13	<1	6	0	0	10	52
195607	0.8	1.7	24.6	-28	0	-7	4	55	-1	13	<1	6	0	9	8	53

TABLE A-5

GUST FRONT CHARACTERISTICS

15 MAY 1982 (cont.)

Time (HHMMSS)	Elevation Angle (deg)	Height (km)	Length (km)	Radial Wind Speed in Outflow (ms^{-1})			Distance from Max Wind to Outflow Boundary (km)	Reflectivity Along Gust Front (dBZ)		Spectrum Width Associated with Gust Front (ms^{-1})			Signal-to-Noise (dB) Threshold	Distance from Gust Front to Generating Storm (km)	Reflectivity ($dBZ \cdot km^{-1}$) Gradient of Generating Storm	Distance from Gust Front to Radar (km)
				Max	Min	Avg		Max	Min	Max	Min	Avg				
195656	1.2	2.4	36.6	-16	0	-7	1	50	-1	9	4	6	0	5	8	55
201348	0.4	0.6	38.2	-13	0	-5	1	11	-1	9	4	6	0	17	5	52
201445	0.8	1.0	25.7	-13	0	-9	1	11	-1	9	4	6	0	18	6	44
201547	1.2	1.1	21.9	-20	0	-5	0	7	-1	9	4	6	0	27	6	42
203352	0.4	0.9	56.6	-11	0	-4	2	11	-1	8	3	6	0	27	2	32

TABLE A-6

GUST FRONT CHARACTERISTICS

30 MAY 1982

Time (HHMMSS)	Elevation Angle (deg)	Height (km)	Length (km)	Radial Wind Speed in Outflow (ms^{-1})			Distance from Max Wind to Outflow Boundary (km)	Reflectivity Along Gust Front (dBZ)		Spectrum Width Associated with Gust Front (ms^{-1})			Signal-to-Noise (dB) Threshold	Distance from Gust Front to Generating Storm (km)	Reflectivity ($dBZ \cdot km^{-1}$) Gradient of Generating Storm	Distance from Gust Front to Radar (km)
				Max	Min	Avg		Max	Min	Max	Min	Avg				
202152	0.5	0.6	24.6	-31	-6	-19	4	45	16	12	<1	7	0	0	2	55
202225	2.0	2.3	13.1	-23	0	-15	8	50	26	11	<1	7	0	0	2	55
202927	0.5	0.6	29.0	-35	-15	-31	10	45	-1	11	2	7	0	0	7	46
203000	2.0	2.0	24.0	-39	-6	-27	5	50	11	11	2	7	0	0	3	48
203034	3.5	3.2	26.2	-35	0	-23	4	50	21	11	1	6	0	0	3	47
203716	0.5	0.3	42.5	-40	-1	-28	2	40	2	13	2	7	0	8	5	33
203849	2.0	1.8	29.8	-36	-7	-28	3	40	11	<15	4	7	0	6	5	39
203919	3.5	2.8	29.1	-36	0	-23	5	41	9	13	2	5	0	6	8	36
204652	0.5	0.5	61.7	-36	0	-23	2	40	-1	11	3	6	0	4	9	25
204722	1.2	1.1	36.6	-32	-7	-23	2	45	-1	13	4	6	0	4	7	26
204752	3.2	2.5	38.1	-32	0	-18	2	50	-1	13	3	7	0	5	7	28

TABLE A-6

GUST FRONT CHARACTERISTICS

30 MAY 1982 (cont.)

Time (HHMMSS)	Elevation Angle (deg)	Height (km)	Length (km)	Radial Wind Speed in Outflow (ms^{-1})			Distance from Max Wind to Outflow Boundary (km)	Reflectivity Along Gust Front (dBZ)		Spectrum Width Associated with Gust Front (ms^{-1})			Signal-to-Noise (dB) Threshold	Distance from Gust Front to Generating Storm (km)	Reflectivity ($dBZ \cdot km^{-1}$) Gradient of Generating Storm	Distance from Gust Front to Radar (km)
				Max	Min	Avg		Max	Min	Max	Min	Avg				
205611	1.2	0.6	35.2	-36	0	-28	2	41	-1	13	2	8	0	8	2	14
205645	3.2	1.7	19.8	-36	0	-23	0	40	-1	13	2	8	0	18	3	15
205714	5.2	1.8	15.1	-23	0	-23	2	41	-1	13	<1	7	0	16	4	14
214017	0.5	0.3	70.1	+18	0	+7	4	11	2	13	2	7	0	40	14	30
214828	0.5	0.5	91.6	+18	0	+7	6	11	2	13	2	7	0	35	14	36
215110	1.3	1.3	80.1	+23	0	+7	5	7	-1	13	2	7	0	39	2	41

TABLE A-7

GUST FRONT CHARACTERISTICS

17 MAY 1983

Time (HHMMSS)	Elevation Angle (deg)	Height (km)	Length (km)	Radial Wind Speed in Outflow (ms^{-1})			Distance from Max Wind to Outflow Boundary (km)	Reflectivity Along Gust Front (dBZ)		Spectrum Width Associated with Gust Front (ms^{-1})			Signal-to-Noise (dB) Threshold	Distance from Gust Front to Generating Storm (km)	Reflectivity ($dBZ \cdot km^{-1}$) Gradient of Generating Storm	Distance from Gust Front to Radar (km)
				Max	Min	Avg		Max	Min	Max	Min	Avg				
222803	0.5	0.5	17.5	-39	-6	-31	3	40	26	11	<1	6	10	4	4	48
222812	0.9	0.9	17.8	-39	-11	-27	4	40	26	11	<1	6	10	3	5	49
222822	1.3	1.3	14.5	-43	-6	-27	4	45	31	11	<1	7	10	2	4	50
222833	1.7	1.7	22.8	-43	-6	-27	3	45	31	11	<1	7	10	5	4	49
222843	2.3	2.3	23.1	-43	-6	-27	3	45	26	11	<1	6	10	5	5	48
223439	0.4	0.4	26.6	-35	-6	-27	2	31	26	11	<1	6	10	4	6	39
223452	0.8	0.7	27.0	-35	-6	-27	2	36	26	11	<1	5	10	4	7	39
223506	1.2	1.0	26.1	-39	-6	-31	1	36	26	11	<1	5	10	4	6	40
223520	2.0	1.7	25.7	-43	-6	-31	1	36	31	11	<1	5	10	4	8	40
224133	0.4	0.2	20.0	-39	-6	-27	3	36	26	11	<1	5	10	5	5	30
224151	0.8	0.4	18.9	-43	-6	-27	4	36	26	11	<1	5	10	5	5	29

TABLE A-7

GUST FRONT CHARACTERISTICS

17 MAY 1983 (cont.)

Time (HHMMSS)	Elevation Angle (deg)	Height (km)	Length (km)	Radial Wind Speed in Outflow (ms^{-1})			Distance from Max Wind to Outflow Boundary (km)	Reflectivity Along Gust Front (dBZ)		Spectrum Width Associated with Gust Front (ms^{-1})			Signal-to-Noise (dB) Threshold	Distance from Gust Front to Generating Storm (km)	Reflectivity ($dBZ \cdot km^{-1}$) Gradient of Generating Storm	Distance from Gust Front to Radar (km)
				Max	Min	Avg		Max	Min	Max	Min	Avg				
224208	1.2	0.7	17.7	-43	-6	-31	2	40	26	11	<1	5	10	5	3	29
224747	0.4	0.2	19.9	-31	0	-27	2	36	26	11	<1	5	10	5	5	24
224758	0.8	0.4	20.4	-43	0	-31	2	40	26	11	<1	5	10	4	4	24
224815	1.2	1.1	12.5	-43	0	-31	4	45	7	11	<1	5	10	4	4	26
225406	0.4	0.1	12.7	-31	-6	-31	1	36	7	11	<1	5	10	4	13	18
225430	0.8	0.2	13.2	-35	-6	-27	1	36	26	11	<1	4	10	3	5	18
225440	1.2	0.4	12.2	-31	-6	-31	1	40	21	11	<1	5	10	4	5	17
230001	0.4	0.0	12.4	-36	-13	-18	2	40	36	8	<1	6	10	3	4	13
230021	0.8	0.1	11.8	-36	-13	-28	2	45	31	8	<1	5	10	4	4	12
230035	1.2	0.3	19.4	-36	-7	-28	2	45	31	8	<1	5	10	4	4	12
230053	3.4	1.2	15.4	-40	-7	-28	2	45	31	8	<1	6	10	2	4	13

TABLE A-7

GUST FRONT CHARACTERISTICS

17 MAY 1983 (cont.)

Time (HHMMSS)	Elevation Angle (deg)	Height (km)	Length (km)	Radial Wind Speed in Outflow (ms^{-1})			Distance from Max Wind to Outflow Boundary (km)	Reflectivity Along Gust Front (dBZ)		Spectrum Width Associated with Gust Front (ms^{-1})			Signal-to-Noise (dB) Threshold	Distance from Gust Front to Generating Storm (km)	Reflectivity ($dBZ \cdot km^{-1}$) Gradient of Generating Storm	Distance from Gust Front to Radar (km)
				Max	Min	Avg		Max	Min	Max	Min	Avg				
230553	0.4	0.0	7.2	-36	-7	-32	1	46	26	8	<1	5	10	3	5	8
230609	0.8	0.0	7.2	-36	-7	-32	1	40	26	8	<1	5	10	3	5	9
230624	1.2	0.1	6.6	-40	-13	-32	1	40	31	*6	<1	5	10	2	5	8
Gust Front At Radar																

TABLE A-8

GUST FRONT CHARACTERISTICS

10 JUNE 1983

Time (HHMMSS)	Elevation Angle (deg)	Height (km)	Length (km)	Radial Wind Speed in Outflow (ms^{-1})			Distance from Max Wind to Outflow Boundary (km)	Reflectivity Along Gust Front (dBZ)		Spectrum Width Associated with Gust Front (ms^{-1})			Signal-to-Noise (dB) Threshold	Distance from Gust Front to Generating Storm (km)	Reflectivity ($dBZ \cdot km^{-1}$) Gradient of Generating Storm	Distance from Gust Front to Radar (km)
				Max	Min	Avg		Max	Min	Max	Min	Avg				
201558	0.4	0.9	14.8	-9	0	-9	0	21	7	9	5	6	0	13	7	90
202817	0.4	0.9	23.4	-16	0	-9	0	40	7	9	4	6	0	8	6	79
203435	0.4	0.9	29.0	-16	-5	-5	0	36	2	7	4	6	0	8	6	74
203501	0.8	1.3	21.6	-16	-5	-13	3	40	16	7	4	6	0	4	3	75
204138	0.8	1.3	26.4	-20	0	-9	0	45	11	9	4	6	0	16	5	70
205839	0.4	0.4	32.1	-16	0	-9	0	11	7	9	2	6	10	19	4	55
210619	0.4	0.4	22.9	-13	0	-7	0	11	11	8	<1	6	15	24	3	47

TABLE A-9

GUST FRONT CHARACTERISTICS

26 APRIL 1984
(First Gust Front)

Time (HHMMSS)	Elevation Angle (deg)	Height (km)	Length (km)	Radial Wind Speed in Outflow (ms^{-1})			Distance from Max Wind to Outflow Boundary (km)	Reflectivity Along Gust Front (dBZ)		Spectrum Width Associated with Gust Front (ms^{-1})			Signal-to-Noise (dB) Threshold	Distance from Gust Front to Generating Storm (km)	Reflectivity ($dBZ \cdot km^{-1}$) Gradient of Generating Storm	Distance from Gust Front to Radar (km)
				Max	Min	Avg		Max	Min	Max	Min	Avg				
202038	0.5	0.9	78.6	-23	-6	-19	3	55	7	11	2	7	10	20	2	57
202122	1.5	2.4	89.4	+19	0	+11	0	55	7	11	2	8	10	19	2	57
202206	2.5	2.7	42.8	+27	0	+15	0	31	16	4	2	2	10	15	1	54
202800	.5	1.1	95.5	-23	-7	-13	5	55	7	13	6	8	10	25	2	45
202851	1.5	2.7	118.1	+18	0	+7	0	55	7	13	3	6	10	25	1	51
222941	2.5	3.6	83.0	+28	0	+13	0	46	11	13	2	5	10	25	1	46
203652	0.5	0.9	97.6	-23	0	-13	5	46	7	13	6	9	10	28	2	42
203731	1.5	1.5	93.3	+32	0	+13	7	46	7	13	3	7	10	28	1	43
204200	0.5	0.7	99.4	-23	0	-13	2	46	7	13	6	8	10	22	2	40
204228	1.5	2.8	100.6	+36	0	+13	2	50	11	13	2	8	10	20	2	40
204657	0.5	1.1	101.6	+28	0	+13	5	46	7	13	6	8	10	20	2	44

TABLE A-9

GUST FRONT CHARACTERISTICS

26 APRIL 1984 (cont.)

Time (HHMMSS)	Elevation Angle (deg)	Height (km)	Length (km)	Radial Wind Speed in Outflow (ms^{-1})			Distance from Max Wind to Outflow Boundary (km)	Reflectivity Along Gust Front (dBZ)		Spectrum Width Associated with Gust Front (ms^{-1})			Signal-to-Noise (dB) Threshold	Distance from Gust Front to Generating Storm (km)	Reflectivity ($dBZ \cdot km^{-1}$) Gradient of Generating Storm	Distance from Gust Front to Radar (km)
				Max	Min	Avg		Max	Min	Max	Min	Avg				
204726	1.5	2.6	96.3	+36	0	+13	6	46	7	13	3	7	10	18	1	38
205155	0.5	0.7	83.7	-18	0	-7	2	46	7	13	6	8	10	20	2	33
205225	1.5	2.0	82.9	+40	0	+7	0	46	11	8	8	8	10	18	2	42
205721	0.5	0.3	56.9	-23	0	-13	4	46	11	13	4	8	0	18	1	29

TABLE A-10

GUST FRONT CHARACTERISTICS

26 APRIL 1984
(Second Gust Front)

Time (HHMMSS)	Elevation Angle (deg)	Height (km)	Length (km)	Radial Wind Speed in Outflow (ms^{-1})			Distance from Max Wind to Outflow Boundary (km)	Reflectivity Along Gust Front (dBZ)		Spectrum Width Associated with Gust Front (ms^{-1})			Signal-to-Noise (dB) Threshold	Distance from Gust Front to Generating Storm (km)	Reflectivity ($dBZ \cdot km^{-1}$) Gradient of Generating Storm	Distance from Gust Front to Radar (km)
				Max	Min	Avg		Max	Min	Max	Min	Avg				
204657	0.5	0.6	11.0	-18	-18	-18	0	7	7	13	6	9	10	8	3	57
205155	0.5	0.7	17.8	-28	-7	-13	1	7	2	13	6	9	10	4	13	48
205721	0.5	0.4	38.6	-28	-7	-18	2	11	7	13	4	9	10	6	16	34
205757	1.5	1.3	30.8	-28	-7	-13	1	40	7	9	4	6	10	5	18	34
210140	0.5	0.6	54.2	-28	-7	-13	2	36	7	13	4	8	10	6	18	29
210204	1.5	1.2	31.9	-32	-7	-13	1	40	7	13	4	9	10	4	26	29
210547	0.5	0.5	48.1	-36	-7	-18	1	40	7	13	4	8	10	8	15	25
210611	1.5	1.1	28.3	-36	-7	-13	0	46	7	13	4	7	10	7	15	24
214810	0.5	0.5	76.6	+28	0	+13	2	16	9	no pattern			0	0	6	19
214946	2.5	1.6	67.6	+36	0	+7	0	40	2	13	2	7	0	0	6	21

TABLE A-10

GUST FRONT CHARACTERISTICS

26 APRIL 1984 (cont.)

Time (HHMMSS)	Elevation Angle (deg)	Height (km)	Length (km)	Radial Wind Speed in Outflow (ms^{-1})			Distance from Max Wind to Outflow Boundary (km)	Reflectivity Along Gust Front (dBZ)		Spectrum Width Associated with Gust Front (ms^{-1})			Signal-to-Noise (dB) Threshold	Distance from Gust Front to Generating Storm (km)	Reflectivity ($dBZ \cdot km^{-1}$) Gradient of Generating Storm	Distance from Gust Front to Radar (km)
				Max	Min	Avg		Max	Min	Max	Min	Avg				
215549	0.0	0.2	94.1	+36	0	+18	5	31	2				0	0	10	25
215701	2.0	1.3	65.3	+36	0	+13	3	50	2	13	4	9	0	0	6	25
220423	0.5	0.5	86.2	+36	0	+13	2	31	2	13	4	9	10	0	6	31

APPENDIX B

Doppler Radial Shear

This appendix contains computed radial shear for three cases:

30 April 1978 (Northern Gust Front)
30 April 1978 (Southern Gust Front)
30 May 1982

Explanations of each of the categories are given below.

Time - beginning time of tilt in hours, minutes and seconds (HHMMSS) CST.

Elevation Angle - elevation angle of the radar antenna in degrees.

Radial Velocity in Outflow - magnitude (ms^{-1}) and radial direction (+ or -) of the maximum, minimum and average radial winds within the outflow in the immediate vicinity of the leading edge.

Radial Shear Along Gust Front - the maximum, minimum and average values of radial shear (10^{-3} s^{-1}) as computed by the NSSL Convergence algorithm.

TABLE B-1

DOPPLER RADIAL SHEAR

30 April 1978

(Northern Gust Front)

Time (HHMMSS)	Elevation Angle (deg)	Radial Velocity in Outflow (ms^{-1})			Radial Shear along Gust Front ($x10^{-3}$ s^{-1})		
		max	min	avg	max	min	avg
202832	0.3	-18	-7	-13	3.19	0.84	1.86
202933	0.7	-18	-7	-13	3.48	1.16	1.93
203034	1.5	-18	0	-13	5.34	1.72	3.08
203134	3.0	-18	-7	-13	5.13	1.14	2.76
204058	0.3	-13	0	-7	3.86	0.85	1.58
204200	0.7	-32	0	-7	4.35	0.74	1.62
204301	1.5	-18	0	-13	5.44	0.95	2.02
204402	3.0	-23	-8	-13	5.72	0.82	2.35
205325	0.3	-28	0	-7	3.10	0.69	1.50
205426	0.7	-18	0	-7	2.11	0.68	1.36
205527	1.5	-18	0	-7	3.21	0.59	1.58
205628	3.0	-18	0	-7	3.05	0.51	1.72
205730	5.0	-18	0	-7	5.27	0.90	2.28
210551	0.3	-23	0	-7	3.24	0.71	1.61
210652	0.7	-18	0	-7	3.79	0.50	1.38
210753	1.5	-23	0	-7	3.34	0.76	1.83
210855	3.0	-23	0	-7	5.10	1.03	2.26
210956	5.0	-28	-7	-13	5.72	1.27	3.27

TABLE B-2

DOPPLER RADIAL SHEAR

30 April 1978

(Southern Gust Front)

Time (HHMMSS)	Elevation Angle (deg)	Radial Velocity in Outflow (ms^{-1})			Radial Shear along Gust Front ($x10^{-3}$ s^{-1})		
		max	min	avg	max	min	avg
202832	0.3	-18	0	-7	not available		
202933	0.7	-18	0	-7	"	"	"
203034	1.5	-28	0	-7	"	"	"
204058	0.3	-28	0	-13	"	"	"
204200	0.7	-28	0	-13	4.45	1.31	2.03
204301	1.5	-28	-7	-18	3.79	1.37	2.67
205325	0.3	-32	0	-18	3.34	1.31	2.02
205426	0.7	-32	0	-18	3.18	1.09	1.84
205527	1.5	-32	0	-18	3.46	0.73	1.73
205628	3.0	-23	-7	-13	6.36	0.67	2.98
205730	5.0	-28	-7	-7	7.54	2.70	4.24
210551	0.2	-28	0	-18	2.97	0.53	1.38
210652	0.7	-28	0	-18	4.25	0.51	1.55
210753	1.5	-32	-7	-18	3.39	1.00	1.93
210855	3.0	-36	0	-18	4.31	0.51	2.10
210956	5.0	-36	-7	-23	4.20	1.25	2.62
211057	7.0	-36	-7	-28	9.47	1.21	3.87

TABLE B-3

DOPPLER RADIAL SHEAR

30 May 1982

Time (HHMMSS)	Elevation Angle (deg)	Radial Velocity in Outflow (ms^{-1})			Radial Shear along Gust Front ($x10^{-3}$ s^{-1})		
		max	min	avg	max	min	avg
202152	0.5	-31	-6	-19	5.24	0.51	2.23
202225	2.0	-23	0	-15	6.29	0.78	3.14
202927	0.5	-35	-15	-31	4.93	0.81	2.76
203000	2.0	-39	-6	-27	7.41	1.08	3.36
203034	3.5	-35	0	-23	1.48	0.52	0.93
203716	0.5	-7	-7	-28	9.42	0.51	3.31
203849	2.0	-36	-7	-28	9.14	1.33	3.83
203919	3.5	-36	0	-23	10.92	1.81	4.88
204652	0.5	-36	0	-23	6.90	0.60	3.65
204722	1.2	-32	-7	-23	7.01	1.56	3.62
204752	3.2	-32	0	-18	7.92	2.22	4.14
205611	1.2	-36	0	-28	6.36	0.70	2.56
205645	3.2	-36	0	-23	12.39	0.76	3.75
205714	5.2	-23	0	-23	5.80	0.71	3.43
214017	0.5	+18	0	+7	4.28	0.50	2.07

APPENDIX C

Interpretation of Radar Displays

Information for proper interpretation of the PPI radar displays is contained in the legend on the right side of each photograph (Fig. C-1). The top two lines are the date and time (CST) of data collection given as month/day/year and hour:minutes:seconds. Color categories (0,1,2,...F) are indicated in units of dBZ (reflectivity display) or ms^{-1} (velocity and spectrum width displays). Category F is reserved for navigation aids and range rings. White squares indicate positions corresponding to cities or locations of particular interest to NSSL (e.g., Cimmaron Doppler Radar, 40 km northwest of Norman, OK). To the right of category F is an "R" followed by a number. This gives the distance between range rings (white arcs on the displays). For instance, "R 40" indicates that the range ring spacing is 40 km.

The bottom one-third of the legend gives information concerning the position of the screen center and cursor. CAZ and CRG are the azimuth and range of the point in the center of the data display relative to the Norman Doppler radar (NRO). The ability to alter this point allows one to center the display on a particular area of interest. SM is the speed and direction of storm motion which is subtracted from the displayed data. AZ+, RG+ and HT+ give the azimuth, range, and height above the surface of the cursor position. (The digit following the cursor range gives the color category for center of cursor.) AZ and EL are azimuth and elevation angle of the radar antenna.

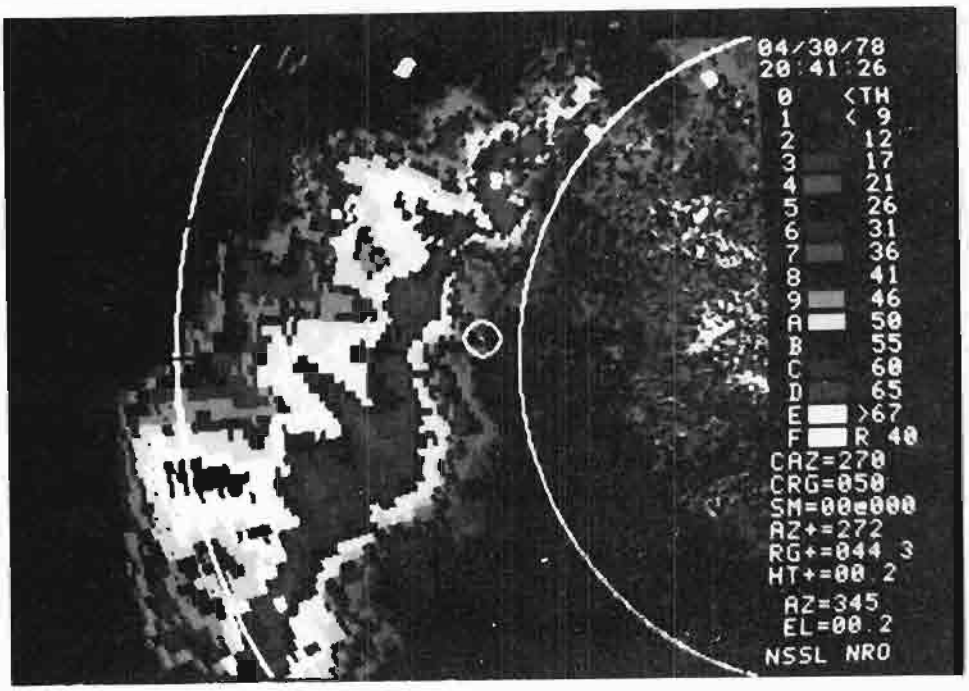

Fig. C-1. Example of the radar reflectivity display. The date and time of this display are 30 April 1978 at 20:41:26 CST. The point at the center of the display has an azimuth of 270° and range of 50 km. No storm motion has been subtracted from the displayed data. The center of the cursor is positioned at an azimuth of 272° and 44 km range. At that range, the center of the beam is 0.2 km above the surface. The reflectivity at the center of the cursor is 17 dBZ (category 3). The radar is pointed at an azimuth of 345° with an elevation angle of 0.2°.

APPENDIX D

Definition of Meteorological Terms

bow echo - A bulge on the forward edge of a line echo. Echoes in the bulge move faster than those near the ends of the line producing an arc or bow shaped echo.

cold front - The leading edge of a relatively cold air mass which moves so that colder air replaces warmer air.

downburst - A strong, small scale downdraft inducing an outward burst of damaging winds on or near the ground. Downbursts are often associated with bow echoes.

downdraft - The cold, dense current of air in a thunderstorm which is produced by evaporative cooling and precipitation drag.

dryline - The leading edge of a relatively dry air mass which moves so that drier air replaces moister air. There is often little temperature contrast across the dryline.

gravity current - The current formed by the intrusion of a dense fluid into an area occupied by a less dense fluid propagates under the force of gravity.

gust front - The leading edge of the thunderstorm outflow produced when the downdraft strikes the surface and spreads out horizontally. It is usually accompanied by an abrupt change in wind speed and/or direction, a rise in pressure, a decrease in temperature and the onset of precipitation.

inversion - A departure from the usual decrease with altitude of atmospheric temperature.

lifted index - A measure of the thermodynamic stability of the atmosphere. A lifted index of ≤ -7 is usually associated with tornadic storms.

low - Low pressure area, or a minimum of atmospheric pressure in two dimensions.

outflow - The cold, dense downdraft air which flows horizontally out of a thunderstorm at the surface.

potential temperature - The temperature a parcel of dry air would have if brought adiabatically from its initial state to the standard pressure of 1000 millibars.

precipitation roll - A reflectivity pattern of precipitation shown by Doppler velocities to be revolving in a horizontal roll at the gust front.

radial shear - Shear of the Doppler velocity that occurs along a radar radial.

radial convergence - Convergence that occurs along a radar radial.

rawinsonde - A method of upper air observation consisting of an evaluation of wind speed and direction, temperature, pressure, and relative humidity aloft by means of a balloon-borne instrument package tracked by radar.

secondary surge - A perturbation or disturbance within the thunderstorm outflow (based on tower data) that exhibits many of the characteristics, in terms of temperature and wind changes, associated with gust front passages.

shear - The variation of a vector field (usually wind) along a given direction in space.

short wave - A progressive wave in the horizontal pattern of air motion having a wavelength of 10^3-10^4 km.

stationary front - A transition zone between two air masses of different characteristics (temperature, moisture, etc.) which has not moved appreciably from its position on the previous weather chart.

streamline - A line whose tangent at any point in a fluid is parallel to the instantaneous velocity of a fluid at that point.

thin line echo - A linear pattern of relatively weak reflectivity often associated with a thunderstorm gust front that has moved away from the main precipitation echo into clear air.

trough - An elongated area of relatively low atmospheric pressure.

upper air disturbance - A disturbance of the flow pattern in the upper air, particularly one which is more strongly developed aloft than near the ground.

veering - A change in wind direction in a clockwise sense (e.g., southeast to southwest to west).

warm front - The leading edge of a relatively warm air mass which moves so that warmer air replaces colder air.